Synaptogyrin-3 mediates presynaptic dysfunction induced by Tau

Neuron

Synaptogyrin-3 mediates presynaptic dysfunction induced by Tau

--Manuscript Draft--

Manuscript Number:	NEURON-D-17-00894R2
Full Title:	Synaptogyrin-3 mediates presynaptic dysfunction induced by Tau
Article Type:	Research Article
Keywords:	Alzheimer's disease; Tauopathy; Tau; presynapse; synaptic vesicles; synaptic dysfunction; Synaptogyrin-3; Syngr3
Corresponding Author:	Patrik Verstreken, PhD K.U.Leuven and VIB Leuven, BELGIUM
First Author:	Joseph McInnes
Order of Authors:	Joseph McInnes
	Keimpe Wierda
	An Snellinx
	Laura Bounti
	Yu-Chun Wang
	Ilie-Cosmin Stancu
	Nuno Apóstolo
	Kris Gevaert
	Ilse Dewachter
	Tara L. Spires-Jones
	Bart De Strooper
	Joris De Wit
	Lujia Zhou
	Patrik Verstreken, PhD
Abstract:	Early synaptic dysfunction is an early pathological feature of neurodegenerative diseases associated with Tau, including Alzheimer's disease. Interfering with early synaptic dysfunction may be therapeutically beneficial to prevent cognitive decline and disease progression, but the mechanisms underlying synaptic defects associated with Tau are unclear. In disease conditions, Tau mislocalizes into pre- and postsynaptic compartments; here, we show that under pathological conditions, Tau binds to presynaptic vesicles in Alzheimer's disease patient brain. We define that the binding of Tau to synaptic vesicles is mediated by the transmembrane vesicle protein Synaptogyrin-3. In fly and mouse models of Tauopathy, reduction of Synaptogyrin-3 prevents the association of presynaptic Tau with vesicles, alleviates Tau-induced defects in vesicle mobility, and restores neurotransmitter release. This work therefore identifies Synaptogyrin-3 as the binding partner of Tau on synaptic vesicles, revealing a new presynapse-specific Tau interactor which may contribute to early synaptic dysfunction in neurodegenerative diseases associated with Tau.
Suggested Reviewers:	Karen H. Ashe, MD, PhD Professor, University of Minnesota hsiao005@umn.edu Expert on Tau mouse models and synaptic functions of Tau
	Mel B. Feany, MD, PhD Professor, Harvard Medical School mel_feany@hms.harvard.edu Expert on Drosophila as a model organism for pathogenic functions of Tau

Highlights

- Pathological Tau accumulates on synaptic vesicles in Alzheimer's disease brain
- Tau binds to synaptic vesicles via the transmembrane protein Synaptogyrin-3
- Synaptogyrin-3 mediates Tau-induced vesicle clustering at presynaptic terminals
- Synaptogyrin-3 reduction restores neurotransmitter release in fly and mouse neurons

eTOC Blurb

Tau mislocalizes to presynaptic terminals in human disease conditions. Here, McInnes et al. show that interaction between Tau and the presynaptic vesicle protein Synaptogyrin-3 restricts synaptic vesicle mobility, driving defects in neurotransmission in fly and mouse models of Tauopathy.

Synaptogyrin-3 mediates presynaptic dysfunction induced by Tau

Joseph McInnes[1,2,8], Keimpe Wierda[1,2], An Snellinx[1,2], Laura Bounti[1,2], Yu-Chun Wang[1,2], Ilie-Cosmin Stancu[3,4], Nuno Apóstolo[1,2], Kris Gevaert[5,6], Ilse Dewachter[3,4], Tara L. Spires-Jones[7], Bart De Strooper[1,2], Joris De Wit[1,2], Lujia Zhou[1,2] and Patrik Verstreken[1,2,9*]

Affiliations:

[1] VIB-KU Leuven Center for Brain & Disease Research,
3000 Leuven, Belgium
[2] Department of Neurosciences and Leuven Brain Institute, KU Leuven
3000 Leuven, Belgium

[3] Institute of Neuroscience, Alzheimer Dementia Group, Catholic University of Louvain,
1200 Brussels, Belgium
[4] Biomedical Research Institute, Hasselt University,
3500 Hasselt, Belgium

[5] VIB-UGent Center for Medical Biotechnology,
9000 Ghent, Belgium
[6] Department of Biochemistry, Ghent University,
9000 Ghent, Belgium

[7] UK Dementia Research Institute, Euan MacDonald Centre, and Centre for Dementia Prevention, Edinburgh Neuroscience, University of Edinburgh,
EH8 9JZ Edinburgh, UK

[8] Present address: Jan and Dan Duncan Neurological Research Institute at Texas Children's Hospital, Baylor College of Medicine, Houston, TX 77030, USA

[9] Lead contact
* Correspondence: patrik.verstreken@kuleuven.vib.be

Keywords: Alzheimer's disease, Tauopathy, Tau, presynapse, synaptic vesicles, synaptic dysfunction, Synaptogyrin-3, Syngr3

Summary

Early synaptic dysfunction is an early pathological feature of neurodegenerative diseases associated with Tau, including Alzheimer's disease. Interfering with early synaptic dysfunction may be therapeutically beneficial to prevent cognitive decline and disease progression, but the mechanisms underlying synaptic defects associated with Tau are unclear. In disease conditions, Tau mislocalizes into pre- and postsynaptic compartments; here, we show that under pathological conditions, Tau binds to presynaptic vesicles in Alzheimer's disease patient brain. We define that the binding of Tau to synaptic vesicles is mediated by the transmembrane vesicle protein Synaptogyrin-3. In fly and mouse models of Tauopathy, reduction of Synaptogyrin-3 prevents the association of presynaptic Tau with vesicles, alleviates Tau-induced defects in vesicle mobility, and restores neurotransmitter release. This work therefore identifies Synaptogyrin-3 as the binding partner of Tau on synaptic vesicles, revealing a new presynapse-specific Tau interactor which may contribute to early synaptic dysfunction in neurodegenerative diseases associated with Tau.

Introduction

Tau pathology is associated with more than twenty neurodegenerative diseases, including Alzheimer's disease (Y. Wang and Mandelkow, 2016). Hyperphosphorylation or mutation of the microtubule-associated protein Tau is common to all of these diseases, collectively termed Tauopathies, and filamentous inclusions of hyperphosphorylated Tau are hallmark pathologies of Alzheimer's disease and other Tauopathies (Ballatore et al., 2007). Tau pathology is not merely a byproduct of other pathological pathways, but is a key mediator of neurotoxicity itself. In mouse models of familial Alzheimer's disease modeling excessive ß-amyloid production, reduction of endogenous Tau ameliorates neurotoxicity and cognitive deficits (Roberson et al., 2007). Moreover, mutations in the Tau-encoding *MAPT* locus are causative of frontotemporal dementia with parkinsonism linked to chromosome 17 (FTDP-17) (Hutton et al., 1998), and Tau duplications or haplotypes which have elevated Tau expression levels are associated with dementia (Allen et al., 2014; Caffrey and Wade-Martins, 2007; Labbé et al., 2016; Le Guennec et al., 2016; Winder-Rhodes et al., 2015). These findings support Tau as an executor of neuronal toxicity and degeneration in human disease.

In physiological conditions, Tau is expressed in neurons and is bound to axonal microtubules. In pathological conditions, however, mutations in Tau (in FTDP-17) or abnormal phosphorylation of Tau (including sporadic Alzheimer's disease) decrease its microtubule binding affinity (Hong et al., 1998; Y. Wang and Mandelkow, 2016), leading to its dissociation from axonal microtubules and subsequent mislocalization to synapses (Spires-Jones and Hyman, 2014; Tai et al., 2012; 2014). In Alzheimer's disease patients and animal models of Tauopathy, Tau mislocalization to synaptic compartments correlates well with the onset of synaptic dysfunction and cognitive decline (DeKosky and Scheff, 1990; Spires-Jones and Hyman, 2014; Yoshiyama et al., 2007). Importantly, synaptic defects are associated with soluble forms of Tau preceding Tau tangle formation in early disease stages (Koss et al., 2016), in agreement with studies showing that soluble Tau is sufficient to drive neuronal dysfunction in the absence of Tau tangles (Crimins et al., 2012; Polydoro et al., 2014; Rocher et al., 2010; Santacruz et al., 2005). These findings highlight a key role of soluble (monomeric or oligomeric) Tau in perturbing synaptic function in early disease stages, which may contribute to subsequent synapse loss and neurodegeneration. However, the mechanisms by which Tau affects synaptic function remain underexplored.

Previous work has elucidated functions of pathological Tau in contributing to postsynaptic dysfunction on account of its mislocalization to dendritic spines and interference with glutamate receptor organization (Hoover et al., 2010; Ittner et al., 2010; Zhao et al., 2016). However, in addition to its postsynaptic localization, pathological Tau is also present in presynaptic compartments (Tai et al., 2014; 2012; Zhou et al., 2017), suggesting that Tau function at the presynapse may also contribute to disease pathogenesis. A presynaptic function of Tau is also

pertinent given that neurodegeneration is thought to begin with loss of presynaptic terminals and proceeds retrograde in a dyeing-back process (Yoshiyama et al., 2007). Moreover, in fly and rat neurons Tau can interfere with neurotransmitter release by associating with synaptic vesicles at presynaptic terminals (Zhou et al., 2017).

In this work, we show that hyperphosphorylated Tau species accumulate on presynaptic vesicles isolated from Alzheimer's disease patient brain, suggesting this pathway contributes to synaptic dysfunction in human disease. Using unbiased proteomic and genetic approaches, we find that the transmembrane synaptic vesicle protein Synaptogyrin-3 mediates the association of Tau with synaptic vesicles *in vitro* and *in vivo*. Reduction of *Drosophila* Synaptogyrin or murine Synaptogyrin-3 levels in neurons from fly and mouse models of Tauopathy reduces the association of Tau with synaptic vesicles, and subsequently rescues Tau-induced defects in vesicle mobility and neurotransmitter release. Our findings identify Synaptogyrin-3 as a novel Tau interactor that mediates Tau-induced synaptic dysfunction, providing important insights into Tau biology and opening new avenues for specifically targeting early presynaptic dysfunction in Tauopathies.

Results

Synaptogyrin-3 is a physical and genetic interactor of Tau

We and others previously described the localization of pathological hyperphosphorylated Tau to presynaptic terminals of Alzheimer's disease patient brains (Tai et al., 2014; 2012; Zhou et al., 2017), and our recent work demonstrated that presynaptically-localized Tau binds to fly and rodent synaptic vesicles (SVs) via its N-terminal domain (Zhou et al., 2017). To assess the possible relevance of Tau association with SVs in human disease, we biochemically fractionated post-mortem brain tissue from Alzheimer's disease patients or non-demented control subjects to isolate SVs (Figures S1A-B). Examining a cohort of 15 patients (Table S1), we observe enrichment of hyperphosphorylated Tau species in the SV fractions from Alzheimer's disease patient brain using antibodies recognizing disease-associated phospho-Tau epitopes (AT8, PHF-1) or total Tau (DAKO) (Figure 1, Figure S1C). We also detect some native Tau on SVs from healthy control subjects, but this amount was on average 2-to-3-fold increased on SVs from Alzheimer's patient brain (Figure 1B, see also Discussion). Furthermore, Tau on SVs from Alzheimer's disease brain are predominantly hyperphosphorylated and oligomeric species, which are known to be highly toxic in the brain (Y. Wang and Mandelkow, 2016). The amount of Tau on SVs was correlated with the diagnosis of Alzheimer's disease but not age (Figure S1D). These data suggest the association of pathological Tau species with SVs in Alzheimer's disease, warranting further exploration of this pathway as a potential contributor to Tau-induced synaptic dysfunction in human disease.

We first determined the binding mechanism of Tau to SVs in order to identify new targets to disrupt this interaction. SVs are comprised of the vesicle membrane, integral transmembrane SV proteins, and peripheral SV-associated proteins (Takamori et al., 2006). We first assessed whether protein-protein interactions or membrane lipid interactions mediate the association of Tau with SVs. We isolated SVs from mouse brain (Figures S2A-B) and performed limited proteolysis by incubation with trypsin, which degrades all peripheral SV-associated proteins and the cytoplasmic domains of transmembrane SV proteins, but leaves the membrane lipid bilayer intact (Figures 2A-B). We then incubated untreated or trypsinized SVs with recombinant human Tau purified from bacteria (Figures S2C-D). Following incubation with Tau, SVs are pelleted by ultracentrifugation and the binding of Tau to SVs is assessed by immunoblotting for Tau in the SV pellet. The co-sedimentation accurately reflects direct Tau binding to SVs and is not influenced by Tau aggregation (Zhou et al., 2017). In the co-sedimentation assay, Tau binds to untreated SVs, but this binding is largely lost upon proteolysis of SV proteins (Figures 2C-D), indicating that SV proteins are required for Tau binding to SVs. Following sedimentation, the amount of Tau in the supernatants is similar, showing that there is no residual trypsin activity following proteolysis of SVs (Figure S2E). In agreement, we also do not detect Tau binding to synthetic protein-free

liposomes which are similar in size and lipid composition to SVs (Figure S2F). Thus, protein-protein interactions underlie the binding of Tau to SVs.

To further delineate whether Tau binds to SVs via interaction with transmembrane SV proteins or peripheral SV-associated proteins, we performed carbonate stripping of SVs. This manipulation removes peripheral SV-associated proteins but leaves transmembrane SV proteins intact (Figure 2E). When introduced into the co-sedimentation assay, Tau binds equally well to untreated and carbonate-stripped SVs (Figures 2F-G), indicating that peripheral SV-associated proteins are dispensable for binding. Together, these data indicate that Tau binds to SVs via interaction with transmembrane SV proteins.

We then utilized an unbiased proteomics approach to identify the transmembrane SV proteins that bind Tau (Figure 3A). We performed high-detergent lysis of isolated SVs to solubilize SV proteins, and performed a co-immunoprecipitation (co-IP) reaction using purified recombinant Tau^{FL}-His or $Tau^{\Delta N}$-His as bait (Figures S2C-D) followed by mass spectrometry analysis to identify bound proteins. The N-terminal domain of Tau is required for binding to SVs (Zhou et al., 2017), and thus the interactor of Tau on SVs should bind full-length Tau (Tau^{FL}) but not N-terminally truncated Tau ($Tau^{\Delta N}$). Using this approach, we identified 8 SV proteins as potential interactors of Tau (Figure 3B, Table S2), but only one protein is both transmembrane and specific to the N-terminus of Tau: Synaptogyrin-3 (Syngr3).

Syngr3 is a SV-specific protein of unknown function that has four transmembrane domains with cytoplasmic exposed N- and C-terminal tails (Kedra et al., 1998). Syngr3 is the only candidate which fits our criteria as a potential interactor of Tau *in vitro*; nevertheless, we tested whether *Drosophila* homologues of any of the 8 SV proteins identified in our proteomics approach show a genetic interaction with Tau *in vivo.* For this, we crossed flies expressing FTDP-17 clinical mutant Tau^{P301L} to loss-of-function alleles or shRNA constructs for the *Drosophila* homologues of these 8 candidate interactors, and we measured colocalization of Tau with SVs as a readout of Tau-SV association *in vivo* (Figures 3C-D). In third-instar *Drosophila* larvae expressing human Tau carrying FTDP-17 clinical mutations (P301L, V337M, or R406W) in motor neurons, mutant Tau dissociates from axonal microtubules and relocalizes to presynaptic boutons at neuromuscular junctions (NMJs). At boutons, Tau colocalizes with SVs that organize in a ring-like pattern in the periphery of the bouton (Figures 4A-B), which is quantified using the Pearson co-localization coefficient between Tau and SVs immunolabeled with anti-Cysteine String Protein (CSP) antibodies. We find that Tau^{P301L} shows a diffuse pattern when we lower the expression level of Synaptogyrin (Syngr, the single *Drosophila* homologue of Syngr3 (R. J. Stevens et al., 2012)), but not any other candidate interactor (Figures 3D, 4A-B). Similarly, two other pathogenic FTDP-17 Tau mutants also show diffuse localization at boutons when Syngr expression is lowered (Figure 4C). Both heterozygous loss (50% reduction) and shRNA-mediated knockdown (90%

reduction, Figures S3A-B) of Syngr were effective to cause dissociation of Tau from SVs to a similar extent as genetically deleting the N-terminal SV binding domain of Tau (expression of $Tau^{\Delta N}$) (Figures 3D, 4A-C), indicating that partial loss of Syngr is sufficient to reduce Tau-SV binding *in vivo* at *Drosophila* NMJs.

To test if Syngr is required for the direct physical interaction of Tau with SVs, we isolated SVs from wildtype (WT) or *syngr* knock-out (KO) adult fly brains (Figures S3C-D). In the co-sedimentation assay, recombinant human Tau binds to WT SVs, but binding to *syngr* KO SVs is severely reduced (Figures 4D-E). These results complement our findings at NMJs *in vivo* where reduction of Syngr caused the diffuse localization of pathogenic Tau (Figures 4A-C). Taken together, these data indicate that the physical interaction between Tau and Syngr is the principle mechanism underlying the binding of Tau to SVs.

Reduction of Synaptogyrin rescues Tau-induced presynaptic dysfunction in *Drosophila*

When Tau binds to SVs they become cross-linked and less mobile, causing defects in the recruitment of a sufficient number of vesicles to maintain neurotransmitter release during sustained activity (Zhou et al., 2017). We show here that Syngr mediates the association of Tau with SVs and we therefore assessed whether reduction of Syngr is sufficient to rescue Tau-induced presynaptic defects. As a readout of SV crosslinking, we examined the mobility of SVs at larval NMJs using a fluorescence recovery after photobleaching (FRAP) assay. In larvae expressing the live SV marker Synaptotagmin-GFP (Syt-GFP), photobleaching of a small area of SVs within a presynaptic bouton depletes those vesicles of Syt-GFP fluorescence, and the recovery of fluorescence signal over time in that area therefore reflects the mobility of other SVs which diffuse in (Seabrooke et al., 2010). In comparison to controls, SV mobility at presynaptic boutons in larvae expressing three independent pathogenic Tau mutants is reduced, indicative of Tau-induced SV crosslinking (Figures 5A-D, solid lines). In contrast, heterozygous loss of Syngr is sufficient to restore SV mobility back to control levels on all three mutant Tau backgrounds (Figures 5A-D, dotted lines). This rescue of SV mobility is specific to pathogenic Tau-induced deficits, as $syngr^{+/-}$ alone on a wildtype background does not affect SV mobility (Figure 5E). Thus, Syngr-dependent binding of Tau to SVs directly impairs SV mobility at presynaptic terminals.

We next assessed whether Syngr mediates Tau-induced defects in neurotransmitter release by acquiring electrophysiological recordings at larval NMJs. Larvae expressing mutant Tau^{P301L} do not show apparent defects in spontaneous release or evoked release in response to short stimuli (Figure S4) but they do show impaired release during sustained activity, exhibiting progressively lower excitatory junction potential (EJP) amplitudes in response to 10 Hz stimulation for 10 minutes (Figures 5F-H, blue). Upon reduction of Syngr levels ($syngr^{+/-}$), however, activity-dependent release is rescued back to control levels (Figures 5F-H, orange). Again, this rescue is specific to pathogenic Tau-induced deficits, as $syngr^{+/-}$ mutant larvae alone

do not exhibit differences in spontaneous or evoked neurotransmitter release during short or sustained stimulation (Figures 5F-H, grey, Figure S4). Taken together, these data support our hypothesis that presynaptically-localized pathogenic Tau directly binds and crosslinks SVs via Syngr, preventing vesicle recruitment into release and ultimately attenuating neurotransmission during sustained activity.

Synaptogyrin-3 mediates presynaptic dysfunction in hippocampal neurons from a Tauopathy mouse model

The mammalian genome encodes four Synaptogyrins which are distantly related to Synaptophysin and Synaptoporin, all of which share a common topology of four transmembrane domains with cytoplasmic exposed N- and C-terminal tails (Kedra et al., 1998). Only Synaptogyrins-1 and -3 are neuron-specific and present on synaptic vesicles (Belizaire et al., 2004). Our proteomics screen only identified Syngr3 as a Tau interactor and we therefore set out to test if reduction of Syngr3 is sufficient to ameliorate synaptic dysfunction in neurons of a well-established transgenic mouse model of Tauopathy. Tau PS19 mice express human FTDP-17 clinical mutant Tau^{P301S} and show disease-relevant features of synaptic dysfunction, synapse loss and neurodegeneration during ageing (Yoshiyama et al., 2007). We first assessed if FTDP-17 mutant Tau^{P301S} localizes to presynaptic terminals in mouse hippocampal neurons. We established primary neuronal cultures from the hippocampi of E17.5 non-transgenic (Non Tg) or Tau PS19 transgenic mouse embryos, allowed them to mature for 17 days in culture, and then assessed Tau^{P301S} localization by immunofluorescence together with the presynaptic markers VGlut1 or Synapsin and the dendritic marker MAP2. Along distal axons, we observe a punctate staining of Tau^{P301S} that colocalizes with VGlut1 (Figures S5A-B), indicative of presynaptic localization; as a control, staining of endogenous mouse Tau (mTau) in Non Tg neurons reveals a more diffusive staining pattern (Figures S5C-D), consistent with predominantly axonal localization. Thus, pathogenic mutant Tau^{P301S} localizes to presynaptic terminals in hippocampal neurons from Tau PS19 mice, recapturing this key pathogenic event also observed in sporadic disease conditions including Alzheimer's disease (Tai et al., 2014; 2012; Zhou et al., 2017).

We then assessed whether lowering the expression level of Syngr3 alters this punctate presynaptic localization of Tau. We produced lentiviruses encoding RFP as well as short hairpin sequences targeting *syngr3* and validated two independent shRNA constructs that result in more than 95% reduction of Syngr3 levels but do not obviously affect neuronal viability, morphology or synapse formation (Figures S5E-H). While Tau^{P301S} maintains its punctate localization to presynaptic SV clusters along the axon in scramble-transduced neurons, knockdown of Syngr3 results in a more diffuse staining pattern of Tau^{P301S} along the axon, with Tau^{P301S} no longer tightly associating with SV clusters (Figure 6A). As a measure of Tau association with presynaptic SV clusters we quantified Tau^{P301S} colocalization with a SV marker along axons, which revealed a

significant reduction in Tau^{P301S} association to presynaptic SV clusters upon Syngr3 knockdown (Figure 6B), whereas overall Tau levels are unaffected (Figure 6C). This reduction in presynaptic localization upon reduction of Syngr3 is specific to Tau PS19 neurons in which Tau^{P301S} has mislocalized to synapses, as reduction of Syngr3 in Non Tg neurons does not affect endogenous mTau localization, consistent with a predominantly axonal localization of native Tau which largely precludes its association with Syngr3 in normal conditions (Figures S5I-J). Together, these data indicate Syngr3-dependent association of presynaptic Tau with SVs in pathogenic conditions.

We next determined whether Syngr3-dependent association of Tau with SVs leads to reduced SV mobility in hippocampal neurons using a SV dispersion assay. At mammalian central synapses, SVs sit in tight clusters along the axon, which become more mobile and diffuse during neuronal activity (Sankaranarayanan and Ryan, 2000). Measuring the change in fluorescence intensity of a live SV marker to assess vesicle diffusion during neuronal stimulation can therefore serve as a measure of SV mobility (L. Wang et al., 2014). We transduced hippocampal neurons with lentivirus expressing the live SV marker Synaptophysin-GFP (Syph-GFP) and performed live imaging to record changes in Syph-GFP fluorescence intensity, which decreases in response to 30 Hz stimulation, reflecting activity-dependent SV mobilization (Figure 6D). In comparison to neurons from Non Tg littermates, neurons from Tau^{P301S} transgenic mice show less dispersion of Syph-GFP fluorescence during 30 Hz stimulation (Figures 6D-E), indicative of impaired SV mobility. However, reducing Syngr3 levels in Tau^{P301S} neurons by transduction with Syngr3 knockdown virus restores SV mobility back to control levels (Figures 6D and 6F). Knockdown of Syngr3 in Non Tg neurons does not affect SV mobility (Figure S5K), therefore the contribution of the Tau-Syngr3 interaction to SV mobility is mostly detected in pathogenic conditions in which Tau has mislocalized to synapses and comes in contact with Syngr3, having a dominant toxic effect on SV mobility. Thus, Syngr3-dependent binding of presynapse-localized Tau to SVs underlies Tau-induced defects in presynaptic vesicle mobility in pathogenic conditions.

Finally, we analyzed whether Tau-induced, Syngr3-mediated defects in SV mobility are functionally related to defects in neurotransmission by performing whole-cell voltage clamp electrophysiology on DIV17-19 autaptic cultures of hippocampal neurons. Tau^{P301S}-expressing neurons show spontaneous release characteristics very similar to those we measure in Non Tg neurons (Figures S6A-C). However, Tau^{P301S} neurons cannot sustain evoked release efficacy as well as controls during high frequency 10 Hz stimulation trains, exhibiting progressively lower eEPSC amplitudes with each stimulation train (Figures 7A-B). Remarkably, reducing Syngr3 levels in Tau^{P301S} neurons by transduction with Syngr3 knockdown virus is sufficient to rescue this evoked neurotransmitter release defect back to control levels (Figures 7A and 7C). This rescue is not due to altered baseline release, as spontaneous release and raw evoked amplitudes among control and rescue genotypes are similar (Figures S6A-D). Furthermore, knockdown of Syngr3 in Non Tg neurons did not affect evoked release during 10 Hz stimulation (Figure S6E), again

suggesting that Syngr3 knockdown specifically rescues Tau-induced deficits in neurotransmitter release under pathogenic conditions in which excessive amounts of Tau have trafficked to the presynaptic terminal. These data support our model that Tau crosslinking SVs via Syngr3 renders a portion of the SV pool unable to be recruited into release, ultimately lowering neurotransmitter release during sustained stimulation.

Taken together, these data identify Syngr3 as a novel interactor of Tau which mediates synaptic release deficits in fly and mouse models of Tauopathy by acting as the binding partner of Tau on SVs. In disease conditions, mutations or hyperphosphorylation of Tau lower its affinity for binding to axonal microtubules, causing mislocalization of Tau into presynaptic terminals where it comes in contact with the SV protein Syngr3, leading to impaired SV mobility and attenuating neurotransmitter release. By targeting Syngr3, an exclusively presynaptic SV protein, we genetically uncouple the presynaptic function of Tau from other potential pathological functions and reveal that specific inhibition of Syngr3-dependent Tau-SV binding ameliorates defects in synaptic function and neurotransmitter release.

Discussion

Synaptic dysfunction is thought to be an early and important pathogenic step in Alzheimer's disease and other neurodegenerative diseases associated with Tau. While accumulating evidence positions Tau itself as a major executor of synaptic dysfunction, the precise mechanisms underlying Tau-induced synaptic pathology have remained elusive. Tau can act postsynaptically, where it affects glutamate receptor trafficking and organization (Hoover et al., 2010; Ittner et al., 2010), as well as presynaptically, where it clusters SVs via F-actin networks (Zhou et al., 2017). Here, we define that Tau binding to the transmembrane SV protein Syngr3 mediates Tau-induced defects in SV mobility, preventing SV recruitment into release and lowering neurotransmission. Given that Syngr3 is exclusively present on SVs, our findings present Syngr3 as a novel Tau interactor involved in Tau pathogenesis at the presynapse. This work opens new avenues for specifically targeting the presynaptic function of Tau both to selectively evaluate the contribution of this pathway to disease progression in animal models, as well as for future therapeutic approaches targeting synaptic dysfunction in Alzheimer's disease and related Tauopathies.

We validated the mechanism of Tau-SV binding as disease relevant by finding that pathological Tau species associate with SVs isolated from Alzheimer's disease patient brains, and used *in vitro* assays of recombinant human Tau binding to isolated SVs to mechanistically define that Tau binds to SVs via interaction with transmembrane SV proteins. Using an unbiased proteomics approach, we identified eight candidate SV interactors, but only Syngr3 was both transmembrane and specific to the N-terminal SV binding domain of Tau and therefore the most likely candidate. Indeed, when we tested the genetic interaction of all eight candidates with Tau in flies, only the Syngr3 homologue reduced Tau association with SVs *in vivo*. In addition, another recent study also identified Syngr3 as a Tau interactor in an unbiased proteomics screen (Liu et al., 2016), independently confirming our result. The identification of other candidate interactors in our screen may be due to secondary interactions with other domains of Tau and could have small contributions to SV binding; nonetheless, our studies identify the interaction between the N-terminus of Tau and Syngr3 to be the predominant mechanism by which Tau associates with SVs. In agreement, loss of only Syngr3 from SVs is sufficient to reduce the associated presynaptic deficits in neurons.

The mammalian genome encodes four Synaptogyrins, but only Syngr1 and Syngr3 are neuron-specific and present on SVs (Belizaire et al., 2004; Kedra et al., 1998). While a redundant role of Syngr1 and Synaptophysin in synaptic plasticity has been described (Janz et al., 1999), the physiological function of Syngr3 remains to be explored. Although its function is unknown, our initial experiments suggest targeting Syngr3 therapeutically may be safe and feasible: >95% knockdown of Synaptogyrin-3 in mouse neurons did not obviously affect neuron or synapse

development, and rescued Tau-induced presynaptic defects without inducing additional toxicity in the parameters we measured. Furthermore, *Drosophila syngr* null KO flies are viable, healthy, and do not show overt defects in presynaptic function (R. J. Stevens et al., 2012). Interestingly, in our fly model a 50% reduction (heterozygous loss) was already sufficient to rescue functional defects, suggesting only mild reduction of Syngr3 may be effective to bring levels of Tau-SV binding below a pathogenic threshold. On one hand, this could be because many non-essential SV proteins are present in low copy number, i.e. 1-3 per SV (Takamori et al., 2006), and lowering Syngr levels by 50% may therefore result in a substantial a pool of SVs devoid of Syngr3. On the other hand, in our current experimental systems the functional effects are rather mild, consistent with other adult-onset neurodegenerative disease phenotypes, and thus reducing this effect by 50% may be sufficient to reduce the effect below a threshold necessary to elicit a detectable effect. Other notable studies could also rescue other Tau phenotypes by heterozygous loss of genetic modifiers (Frost et al., 2014; Lasagna-Reeves et al., 2016). While the future identification of inhibitors blocking the Tau-Syngr3 interaction could be useful to titrate the amount of inhibition necessary to rescue functional deficits, the current dataset suggests that partial inhibition the Tau-Syngr3 interaction may be a feasible and relatively safe therapeutic avenue to pursue.

It is worth noting that wildtype, mutant and hyperphosphorylated Tau all have identical N-terminal SV binding domains and therefore equal binding affinity to SVs (Zhou et al., 2017); however, it is the pathogenic condition which drives excess Tau to the presynaptic terminal and therefore gives it the opportunity to bind SVs/Syngr3, eliciting dominant toxic effects on SV mobility. Given the conservation and specificity of the interaction between Tau and Syngr3, and the observation that some Tau is recovered on SVs from healthy control subjects (Figure 1), it is tempting to speculate that a native interaction between endogenous Tau and Syngr3 may have a physiological function in SV clustering as well. However, our experiments thus far analyzing SV mobility and evoked neurotransmitter release upon reduction of Tau (Zhou et al., 2017) or Syngr3 (this study) in wildtype neurons did not reveal a detectable effect, although this does not exclude the possibility of a physiological function of native Tau in SV clustering. It is possible that the loss of Tau or Syngr3 is compensated for by other SV clustering proteins, or that a native role for the Tau-Syngr3 in SV clustering is too subtle to be detected in our experimental paradigms. It is also noteworthy that we observe mostly oligomeric Tau species on SVs from Alzheimer's disease patients, which could potentially be more neurotoxic by simultaneously binding multiple SVs, amplifying the effect of Tau on SV clustering. While a potential physiological function of Tau and Syngr3 should be further investigated, the current dataset is consistent with a primarily gain-of-toxic-function mechanism in which Tau mutations or phosphorylation in disease conditions drive the excessive presynaptic localization of Tau, thus allowing it to interact with Syngr3/SVs to elicit presynaptic functional deficits.

Finally, several observations make Syngr3 interesting as a potentially disease-relevant Tau interactor. First, while expressed throughout the brain, Syngr3 expression is enriched in the hippocampus (Belizaire et al., 2004), a region particularly vulnerable to neuronal dysfunction in Alzheimer's disease and Tauopathy mouse models (H. Braak and E. Braak, 1991; Yoshiyama et al., 2007). Second, Syngr3 levels are 4-fold higher on glutamatergic SVs compared to GABAergic SVs (Bragina et al., 2010), consistent with a recent report showing that early Tau pathology preferentially affects excitatory neurons (Fu et al., 2017). Third, Syngr3 is also present on extracellular vesicles (Gallart-Palau et al., 2016), which have been proposed as vehicles of cell-to-cell transfer of pathological Tau species spreading throughout the brain (H. Braak and E. Braak, 1991; de Calignon et al., 2012; Pickett et al., 2017), a process which is also synapse- and activity-dependent (Calafate et al., 2015; Thompson et al., 2016; Wu et al., 2016). While these connections are only speculative, they nonetheless poise Syngr3 as an interesting and potentially relevant interactor of Tau warranting further investigation. Importantly, perturbations in synaptic function associated with Tau are thought to drive disease progression but the contribution of the presynaptic role of Tau has never been tested experimentally due to lack of a specific approach. Therefore, the identification of Syngr3, an exclusively presynaptic SV protein, provides a new way to assess the contribution of the presynaptic role of Tau to overall neuronal dysfunction, independent of other pathways such as Tau aggregation or Tau localization to post-synapses.

In summary, we uncovered the interaction of Tau with the SV protein Syngr3 as the principle mechanism of Tau binding to presynaptic vesicles, a key step which leads to excessive Tau-induced SV clustering, resulting in restricted SV mobility and ultimately attenuating neurotransmission. Syngr3 is therefore a new culprit in Tau pathogenesis, opening an avenue for the specific targeting of Tau synaptotoxicity in early stages of synaptic and cognitive dysfunction in Alzheimer's disease and related Tauopathies.

Author Contributions

J.M., L.Z. and P.V. conceived the study, designed experiments, analyzed data and wrote the manuscript. K.W. designed, performed and analyzed electrophysiology on hippocampal neurons. L.Z. performed electrophysiology at NMJs. J.M. performed all other experiments. A.S., L.B., Y.W., I.S. and N.A. assisted with experiments. K.G. supervised mass spectrometry experiments. T.L.S.-J. provided human tissue samples. I.D., B.D.S. and J.D.W. contributed to study design, analysis of the data, and providing reagents. All authors edited the manuscript and approved the final version.

Acknowledgements

We thank the members of the Verstreken, De Wit and De Strooper labs for advice. We thank J. Pauwels and F. Impens (VIB Proteomics Core) and K. Vennekens, K. Horré, K. Craessaerts, V. Hendrickx, and J. Verwaeren for assistance. We thank J. T. Littleton for Synaptogyrin knock-out flies and antibodies. We gratefully acknowledge the patient donors and their families and thank the MRC Edinburgh Brain and Tissue bank. This work was supported by ERC CoG grants, the IWT, the Interuniversity Attraction Pole program by BELSPO, a Methusalem grant of the Flemish government, Opening the Future (LUF), the Fonds voor Wetenschappelijk Onderzoek Vlaanderen (FWO), the UK Dementia Research Institute (Medical Research Council, Alzheimer's Society, and Alzheimer's Research UK), and VIB. J.D.W. is supported by an ERC Starting Grant and a FWO Odysseus grant. P.V. and T.L.S.-J. are members of the FENS Kavli Network of Excellence.

Declaration of Interests

The authors declare no conflict of interest.

References

Ahmed, S., Holt, M., Riedel, D., Jahn, R., 2013. Small-scale isolation of synaptic vesicles from mammalian brain. Nat Protoc 8, 998–1009. doi:10.1038/nprot.2013.053

Allen, M., Kachadoorian, M., Quicksall, Z., Zou, F., Chai, H.S., Younkin, C., Crook, J.E., Pankratz, V.S., Carrasquillo, M.M., Krishnan, S., Nguyen, T., Ma, L., Malphrus, K., Lincoln, S., Bisceglio, G., Kolbert, C.P., Jen, J., Mukherjee, S., Kauwe, J.K., Crane, P.K., Haines, J.L., Mayeux, R., Pericak-Vance, M.A., Farrer, L.A., Schellenberg, G.D., Parisi, J.E., Petersen, R.C., Graff-Radford, N.R., Dickson, D.W., Younkin, S.G., Ertekin-Taner, N., 2014. Association of MAPT haplotypes with Alzheimer's disease risk and MAPT brain gene expression levels. Alzheimers Res Ther 6, 39. doi:10.1186/alzrt268

Ballatore, C., Lee, V.M., Trojanowski, J.Q., 2007. Tau-mediated neurodegeneration in Alzheimer's disease and related disorders. Nature Reviews Neuroscience 8, 663–672. doi:10.1038/nrn2194

Bekkers, J.M., Stevens, C.F., 1991. Excitatory and inhibitory autaptic currents in isolated hippocampal neurons maintained in cell culture. Proc. Natl. Acad. Sci. U.S.A. 88, 7834–7838.

Belizaire, R., Komanduri, C., Wooten, K., Chen, M., Thaller, C., Janz, R., 2004. Characterization of synaptogyrin 3 as a new synaptic vesicle protein. J. Comp. Neurol. 470, 266–281. doi:10.1002/cne.20008

Bigay, J., Casella, J.-F., Drin, G., Mesmin, B., Antonny, B., 2005. ArfGAP1 responds to membrane curvature through the folding of a lipid packing sensor motif. EMBO J. 24, 2244–2253. doi:10.1038/sj.emboj.7600714

Braak, H., Braak, E., 1991. Neuropathological stageing of Alzheimer-related changes. Acta Neuropathol 82, 239–259. doi:10.1007/BF00308809

Bragina, L., Giovedì, S., Barbaresi, P., Benfenati, F., Conti, F., 2010. Heterogeneity of glutamatergic and GABAergic release machinery in cerebral cortex: analysis of synaptogyrin, vesicle-associated membrane protein, and syntaxin. Neuroscience 165, 934–943. doi:10.1016/j.neuroscience.2009.11.009

Brose, N., Hofmann, K., Hata, Y., Sudhof, T.C., 1995. Mammalian homologues of Caenorhabditis elegans unc-13 gene define novel family of C2-domain proteins. J. Biol. Chem. 270, 25273–25280.

Burgalossi, A., Jung, S., Man, K.-N.M., Nair, R., Jockusch, W.J., Wojcik, S.M., Brose, N., Rhee, J.-S., 2012. Analysis of neurotransmitter release mechanisms by photolysis of caged Ca^{2+} in an autaptic neuron culture system. Nat Protoc 7, 1351–1365. doi:10.1038/nprot.2012.074

Burré, J., Beckhaus, T., Schägger, H., Corvey, C., Hofmann, S., Karas, M., Zimmermann, H., Volknandt, W., 2006. Analysis of the synaptic vesicle proteome using three gel-based protein separation techniques. Proteomics 6, 6250–6262. doi:10.1002/pmic.200600357

Caffrey, T.M., Wade-Martins, R., 2007. Functional MAPT haplotypes: bridging the gap between genotype and neuropathology. Neurobiol. Dis. 27, 1–10. doi:10.1016/j.nbd.2007.04.006

Calafate, S., Buist, A., Miskiewicz, K., Vijayan, V., Daneels, G., De Strooper, B., De Wit, J., Verstreken, P., Moechars, D., 2015. Synaptic Contacts Enhance Cell-to-Cell Tau Pathology Propagation. Cell Rep 11, 1176–1183. doi:10.1016/j.celrep.2015.04.043

Crimins, J.L., Rocher, A.B., Luebke, J.I., 2012. Electrophysiological changes precede morphological changes to frontal cortical pyramidal neurons in the rTg4510 mouse model of progressive tauopathy. Acta Neuropathol 124, 777–795. doi:10.1007/s00401-012-1038-9

de Calignon, A., Polydoro, M., Suárez-Calvet, M., William, C., Adamowicz, D.H., Kopeikina, K.J., Pitstick, R., Sahara, N., Ashe, K.H., Carlson, G.A., Spires-Jones, T.L., Hyman, B.T., 2012. Propagation of tau pathology in a model of early Alzheimer's disease. Neuron 73, 685–697. doi:10.1016/j.neuron.2011.11.033

DeKosky, S.T., Scheff, S.W., 1990. Synapse loss in frontal cortex biopsies in Alzheimer's disease: correlation with cognitive severity. Ann. Neurol. 27, 457–464. doi:10.1002/ana.410270502

Depner, H., Lützkendorf, J., Babkir, H.A., Sigrist, S.J., Holt, M.G., 2014. Differential centrifugation-based biochemical fractionation of the Drosophila adult CNS. Nat Protoc 9, 2796–2808. doi:10.1038/nprot.2014.192

DiAntonio, A., Parfitt, K.D., Schwarz, T.L., 1993. Synaptic transmission persists in synaptotagmin mutants of Drosophila. Cell 73, 1281–1290.

Frost, B., Hemberg, M., Lewis, J., Feany, M.B., 2014. Tau promotes neurodegeneration through global chromatin relaxation. Nat. Neurosci. 17, 357–366. doi:10.1038/nn.3639

Fu, H., Rodriguez, G.A., Herman, M., Emrani, S., Nahmani, E., Barrett, G., Figueroa, H.Y., Goldberg, E., Hussaini, S.A., Duff, K.E., 2017. Tau Pathology Induces Excitatory Neuron Loss, Grid Cell Dysfunction, and Spatial Memory

Deficits Reminiscent of Early Alzheimer's Disease. Neuron 93, 533–541.e5. doi:10.1016/j.neuron.2016.12.023
Gallart-Palau, X., Serra, A., Sze, S.K., 2016. Enrichment of extracellular vesicles from tissues of the central nervous system by PROSPR. Mol Neurodegener 11, 41. doi:10.1186/s13024-016-0108-1
Hong, M., Zhukareva, V., Vogelsberg-Ragaglia, V., Wszolek, Z., Reed, L., Miller, B.I., Geschwind, D.H., Bird, T.D., McKeel, D., Goate, A., Morris, J.C., Wilhelmsen, K.C., Schellenberg, G.D., Trojanowski, J.Q., Lee, V.M., 1998. Mutation-specific functional impairments in distinct tau isoforms of hereditary FTDP-17. Science 282, 1914–1917. doi:10.1126/science.282.5395.1914
Hoover, B.R., Reed, M.N., Su, J., Penrod, R.D., Kotilinek, L.A., Grant, M.K., Pitstick, R., Carlson, G.A., Lanier, L.M., Yuan, L.-L., Ashe, K.H., Liao, D., 2010. Tau mislocalization to dendritic spines mediates synaptic dysfunction independently of neurodegeneration. Neuron 68, 1067–1081. doi:10.1016/j.neuron.2010.11.030
Hutton, M., Lendon, C.L., Rizzu, P., Baker, M., Froelich, S., Houlden, H., Pickering-Brown, S., Chakraverty, S., Isaacs, A., Grover, A., Hackett, J., Adamson, J., Lincoln, S., Dickson, D., Davies, P., Petersen, R.C., Stevens, M., de Graaff, E., Wauters, E., van Baren, J., Hillebrand, M., Joosse, M., Kwon, J.M., Nowotny, P., Che, L.K., Norton, J., Morris, J.C., Reed, L.A., Trojanowski, J., Basun, H., Lannfelt, L., Neystat, M., Fahn, S., Dark, F., Tannenberg, T., Dodd, P.R., Hayward, N., Kwok, J.B., Schofield, P.R., Andreadis, A., Snowden, J., Craufurd, D., Neary, D., Owen, F., Oostra, B.A., Hardy, J., Goate, A., van Swieten, J., Mann, D., Lynch, T., Heutink, P., 1998. Association of missense and 5'-splice-site mutations in tau with the inherited dementia FTDP-17. Nature 393, 702–705. doi:10.1038/31508
Ittner, L.M., Ke, Y.D., Delerue, F., Bi, M., Gladbach, A., van Eersel, J., Wölfing, H., Chieng, B.C., Christie, M.J., Napier, I.A., Eckert, A., Staufenbiel, M., Hardeman, E., Götz, J., 2010. Dendritic function of tau mediates amyloid-beta toxicity in Alzheimer's disease mouse models. Cell 142, 387–397. doi:10.1016/j.cell.2010.06.036
Janz, R., Sudhof, T.C., Hammer, R.E., Unni, V., Siegelbaum, S.A., Bolshakov, V.Y., 1999. Essential roles in synaptic plasticity for synaptogyrin I and synaptophysin I. Neuron 24, 687–700. doi:10.1016/S0896-6273(00)81122-8
Kasprowicz, J., Kuenen, S., Swerts, J., Miskiewicz, K., Verstreken, P., 2014. Dynamin photoinactivation blocks Clathrin and α-adaptin recruitment and induces bulk membrane retrieval. J Cell Biol 204, 1141–1156. doi:10.1083/jcb.201310090
Kedra, D., Pan, H.Q., Seroussi, E., Fransson, I., Guilbaud, C., Collins, J.E., Dunham, I., Blennow, E., Roe, B.A., Piehl, F., Dumanski, J.P., 1998. Characterization of the human synaptogyrin gene family. Hum. Genet. 103, 131–141. doi:10.1007/s004390050795
Koss, D.J., Jones, G., Cranston, A., Gardner, H., Kanaan, N.M., Platt, B., 2016. Soluble pre-fibrillar tau and β-amyloid species emerge in early human Alzheimer's disease and track disease progression and cognitive decline. Acta Neuropathol 132, 875–895. doi:10.1007/s00401-016-1632-3
Labbé, C., Heckman, M.G., Lorenzo-Betancor, O., Soto-Ortolaza, A.I., Walton, R.L., Murray, M.E., Allen, M., Uitti, R.J., Wszolek, Z.K., Smith, G.E., Kantarci, K., Knopman, D.S., Lowe, V.J., Jack, C.R., Ertekin-Taner, N., Hassan, A., Savica, R., Petersen, R.C., Parisi, J.E., Maraganore, D.M., Graff-Radford, N.R., Ferman, T.J., Boeve, B.F., Dickson, D.W., Ross, O.A., 2016. MAPT haplotype H1G is associated with increased risk of dementia with Lewy bodies. Alzheimers Dement 12, 1297–1304. doi:10.1016/j.jalz.2016.05.002
Lasagna-Reeves, C.A., de Haro, M., Hao, S., Park, J., Rousseaux, M.W.C., Al-Ramahi, I., Jafar-Nejad, P., Vilanova-Velez, L., See, L., De Maio, A., Nitschke, L., Wu, Z., Troncoso, J.C., Westbrook, T.F., Tang, J., Botas, J., Zoghbi, H.Y., 2016. Reduction of Nuak1 Decreases Tau and Reverses Phenotypes in a Tauopathy Mouse Model. Neuron 92, 407–418. doi:10.1016/j.neuron.2016.09.022
Le Guennec, K., Quenez, O., Nicolas, G., Wallon, D., Rousseau, S., Richard, A.-C., Alexander, J., Paschou, P., Charbonnier, C., Bellenguez, C., Grenier-Boley, B., Lechner, D., Bihoreau, M.-T., Olaso, R., Boland, A., Meyer, V., Deleuze, J.-F., Amouyel, P., Munter, H.M., Bourque, G., Lathrop, M., Frebourg, T., Redon, R., Letenneur, L., Dartigues, J.-F., Martinaud, O., Kalev, O., Mehrabian, S., Traykov, L., Ströbel, T., Le Ber, I., Caroppo, P., Epelbaum, S., Jonveaux, T., Pasquier, F., Rollin-Sillaire, A., Génin, E., Guyant-Maréchal, L., Kovacs, G.G., Lambert, J.-C., Hannequin, D., Campion, D., Rovelet-Lecrux, A., 2016. 17q21.31 duplication causes prominent tau-related dementia with increased MAPT expression. Molecular Psychiatry 1–7. doi:10.1038/mp.2016.226
Liu, C., Song, X., Nisbet, R., Götz, J., 2016. Co-immunoprecipitation with Tau Isoform-specific Antibodies Reveals Distinct Protein Interactions and Highlights a Putative Role for 2N Tau in Disease. J. Biol. Chem. 291, 8173–8188. doi:10.1074/jbc.M115.641902
Piccoli, G., Onofri, F., Cirnaru, M.D., Kaiser, C.J.O., Jagtap, P., Kastenmüller, A., Pischedda, F., Marte, A., Zweydorf, von, F., Vogt, A., Giesert, F., Pan, L., Antonucci, F., Kiel, C., Zhang, M., Weinkauf, S., Sattler, M., Sala, C.,

Matteoli, M., Ueffing, M., Gloeckner, C.J., 2014. Leucine-rich repeat kinase 2 binds to neuronal vesicles through protein interactions mediated by its C-terminal WD40 domain. Mol. Cell. Biol. 34, 2147–2161. doi:10.1128/MCB.00914-13

Pickett, E.K., Henstridge, C.M., Allison, E., Pitstick, R., Pooler, A., Wegmann, S., Carlson, G., Hyman, B.T., Spires-Jones, T.L., 2017. Spread of tau down neural circuits precedes synapse and neuronal loss in the rTgTauEC mouse model of early Alzheimer's disease. Synapse 71. doi:10.1002/syn.21965

Polydoro, M., Dzhala, V.I., Pooler, A.M., Nicholls, S.B., McKinney, A.P., Sanchez, L., Pitstick, R., Carlson, G.A., Staley, K.J., Spires-Jones, T.L., Hyman, B.T., 2014. Soluble pathological tau in the entorhinal cortex leads to presynaptic deficits in an early Alzheimer's disease model. Acta Neuropathol 127, 257–270. doi:10.1007/s00401-013-1215-5

Roberson, E.D., Scearce-Levie, K., Palop, J.J., Yan, F., Cheng, I.H., Wu, T., Gerstein, H., Yu, G.-Q., Mucke, L., 2007. Reducing endogenous tau ameliorates amyloid beta-induced deficits in an Alzheimer's disease mouse model. Science 316, 750–754. doi:10.1126/science.1141736

Rocher, A.B., Crimins, J.L., Amatrudo, J.M., Kinson, M.S., Todd-Brown, M.A., Lewis, J., Luebke, J.I., 2010. Structural and functional changes in tau mutant mice neurons are not linked to the presence of NFTs. Exp. Neurol. 223, 385–393. doi:10.1016/j.expneurol.2009.07.029

Sankaranarayanan, S., Ryan, T.A., 2000. Real-time measurements of vesicle-SNARE recycling in synapses of the central nervous system. Nature Cell Biology 2, 197–204. doi:10.1038/35008615

Santacruz, K., Lewis, J., Spires, T., Paulson, J., Kotilinek, L., Ingelsson, M., Guimaraes, A., DeTure, M., Ramsden, M., McGowan, E., Forster, C., Yue, M., Orne, J., Janus, C., Mariash, A., Kuskowski, M., Hyman, B., Hutton, M., Ashe, K.H., 2005. Tau suppression in a neurodegenerative mouse model improves memory function. Science 309, 476–481. doi:10.1126/science.1113694

Seabrooke, S., Qiu, X., Stewart, B.A., 2010. Nonmuscle Myosin II helps regulate synaptic vesicle mobility at the Drosophila neuromuscular junction. BMC Neurosci 11, 37. doi:10.1186/1471-2202-11-37

Spires-Jones, T.L., Hyman, B.T., 2014. The intersection of amyloid beta and tau at synapses in Alzheimer's disease. Neuron 82, 756–771. doi:10.1016/j.neuron.2014.05.004

Stevens, R.J., Akbergenova, Y., Jorquera, R.A., Littleton, J.T., 2012. Abnormal synaptic vesicle biogenesis in Drosophila synaptogyrin mutants. J. Neurosci. 32, 18054–67– 18067a. doi:10.1523/JNEUROSCI.2668-12.2012

Tai, H.-C., Serrano-Pozo, A., Hashimoto, T., Frosch, M.P., Spires-Jones, T.L., Hyman, B.T., 2012. The synaptic accumulation of hyperphosphorylated tau oligomers in Alzheimer disease is associated with dysfunction of the ubiquitin-proteasome system. Am. J. Pathol. 181, 1426–1435. doi:10.1016/j.ajpath.2012.06.033

Tai, H.-C., Wang, B.Y., Serrano-Pozo, A., Frosch, M.P., Spires-Jones, T.L., Hyman, B.T., 2014. Frequent and symmetric deposition of misfolded tau oligomers within presynaptic and postsynaptic terminals in Alzheimer's disease. Acta Neuropathol Commun 2, 146. doi:10.1186/s40478-014-0146-2

Takamori, S., Holt, M., Stenius, K., Lemke, E.A., Grønborg, M., Riedel, D., Urlaub, H., Schenck, S., Brügger, B., Ringler, P., Müller, S.A., Rammner, B., Gräter, F., Hub, J.S., De Groot, B.L., Mieskes, G., Moriyama, Y., Klingauf, J., Grubmüller, H., Heuser, J., Wieland, F., Jahn, R., 2006. Molecular anatomy of a trafficking organelle. Cell 127, 831–846. doi:10.1016/j.cell.2006.10.030

Thompson, A.G., Gray, E., Heman-Ackah, S.M., Mäger, I., Talbot, K., Andaloussi, S.E., Wood, M.J., Turner, M.R., 2016. Extracellular vesicles in neurodegenerative disease - pathogenesis to biomarkers. Nat Rev Neurol 12, 346–357. doi:10.1038/nrneurol.2016.68

Verstreken, P., Koh, T.-W., Schulze, K.L., Zhai, R.G., Hiesinger, P.R., Zhou, Y., Mehta, S.Q., Cao, Y., Roos, J., Bellen, H.J., 2003. Synaptojanin is recruited by endophilin to promote synaptic vesicle uncoating. Neuron 40, 733–748. doi:10.1038/nrn1315

Wang, L., Das, U., Scott, D.A., Tang, Y., McLean, P.J., Roy, S., 2014. α-synuclein multimers cluster synaptic vesicles and attenuate recycling. Curr. Biol. 24, 2319–2326. doi:10.1016/j.cub.2014.08.027

Wang, Y., Mandelkow, E., 2016. Tau in physiology and pathology. Nat. Rev. Neurosci. 17, 5–21. doi:10.1038/nrn.2015.1

Winder-Rhodes, S.E., Hampshire, A., Rowe, J.B., Peelle, J.E., Robbins, T.W., Owen, A.M., Barker, R.A., 2015. Association between MAPT haplotype and memory function in patients with Parkinson's disease and healthy aging individuals. Neurobiol. Aging 36, 1519–1528. doi:10.1016/j.neurobiolaging.2014.12.006

Wu, J.W., Hussaini, S.A., Bastille, I.M., Rodriguez, G.A., Mrejeru, A., Rilett, K., Sanders, D.W., Cook, C., Fu, H., Boonen, R.A.C.M., Herman, M., Nahmani, E., Emrani, S., Figueroa, Y.H., Diamond, M.I., Clelland, C.L., Wray, S.,

Duff, K.E., 2016. Neuronal activity enhances tau propagation and tau pathology in vivo. Nat. Neurosci. 19, 1085–1092. doi:10.1038/nn.4328

Yoshiyama, Y., Higuchi, M., Zhang, B., Huang, S.-M., Iwata, N., Saido, T.C., Maeda, J., Suhara, T., Trojanowski, J.Q., Lee, V.M.Y., 2007. Synapse loss and microglial activation precede tangles in a P301S tauopathy mouse model. Neuron 53, 337–351. doi:10.1016/j.neuron.2007.01.010

Zhao, X., Kotilinek, L.A., Smith, B., Hlynialuk, C., Zahs, K., Ramsden, M., Cleary, J., Ashe, K.H., 2016. Caspase-2 cleavage of tau reversibly impairs memory. Nat. Med. 22, 1268–1276. doi:10.1038/nm.4199

Zhou, L., McInnes, J., Wierda, K., Holt, M., Herrmann, A.G., Jackson, R.J., Wang, Y.-C., Swerts, J., Beyens, J., Miskiewicz, K., Vilain, S., Dewachter, I., Moechars, D., De Strooper, B., Spires-Jones, T.L., De Wit, J., Verstreken, P., 2017. Tau association with synaptic vesicles causes presynaptic dysfunction. Nature Communications 8, 1–13. doi:10.1038/ncomms15295

Figure Legends

Figure 1. Pathological Tau species accumulate on synaptic vesicles isolated from Alzheimer's disease patient brains. SVs were isolated from post-mortem brain tissue of control subjects or Alzheimer's disease (AD) patients and assessed for total Tau levels (DAKO antibody) and phospho-Tau (pTau) levels using the AT8 antibody (phospho-Ser^{202}/Thr^{205} epitope) or PHF-1 antibody (phospho-Ser^{396}/Ser^{404} epitope) by immunoblotting. (A) Representative immunoblots directly comparing the amount of pTau and total Tau in total homogenates and SV fractions from AD patients or controls. Note the presence of both monomeric (around 50 kDa) as well as oligomeric ($\geq$ 100 kDa) Tau/pTau species accumulating on SVs in AD patient brain. GAPDH and Synaptotagmin-1 (Syt) are used as loading controls for total homogenates and SV fractions, respectively. (B) Quantifications of immunoblots comparing pTau or total Tau levels in control and AD patient brain in either total homogenate or SV fractions, normalized to loading controls. Graphs depict mean ± SEM (n = 13 non-demented control subjects, n = 15 AD patients, Student's t-test, ns – not significant, ** $p < 0.01$, *** $p < 0.001$). See also Figure S1 and Table S1.

Figure 2. Tau binds to synaptic vesicles via interaction with transmembrane synaptic vesicle proteins. (A) Ponceau S staining of fractions taken during trypsin digestion of SVs shows proteolysis of SV proteins by trypsin. (B) Immunoblotting of trypsinized SVs shows proteolytic degradation of the SV-associated proteins Synapsin (Syn) and Munc18, and degradation of the cytoplasmic domains of the transmembrane SV proteins SV2, Synaptobrevin-2 (Syb) (cytoplasmic epitopes) and Synaptotagmin-1 (Syt) (intravesicular epitope). (C) Representative immunoblots from co-sedimentation assay with purified recombinant human Tau-His and untreated or trypsinized SVs. Immunoblotting for Tau (anti-His antibody) in the SV pellet assesses binding to SVs as quantified in (D). Graph depicts mean ± SD (n = 3 experiments, Student's t-test, *** $p < 0.001$). (E) Immunoblotting of untreated or carbonate-stripped SVs confirms removal of the SV-associated proteins Syn and Munc18 but retention of the transmembrane SV proteins SV2, Syb and Syt (cytoplasmic epitopes). (F) Representative immunoblots from co-sedimentation assay assessing Tau binding to untreated or carbonate-stripped SVs as quantified in (G). Graph depicts mean ± SD from two independent experiments. See also Figure S2.

Figure 3. Integrated proteomic and genetic screens identify Synaptogyrin-3 as a physical and genetic interactor of Tau. (A-B) Identification of the SV interactor of Tau by mass spectrometry. (A) Experimental workflow of co-IP of SV protein lysate with purified recombinant human Tau. (B) Filtered results from LC-MS/MS analysis showing peptide counts from three replicates. Proteins specific to the N-terminus of Tau are in red. See also Table S2 for raw dataset. (C-D) *In vivo* follow-up screen of candidate interactors in *Drosophila*. (C) Experimental workflow to assess Tau binding to SVs (as measured by colocalization of Tau with SVs) at NMJs upon loss of candidate interactors identified in (B). (D) Quantification of relative colocalization of immunolabeled Tau

and the SV marker CSP at NMJs (see Figure 4). *Drosophila* larvae express UAS-Tau^{P301L} or UAS-Tau^{P301L} ΔN under the motor neuron-specific D42-Gal4 driver. Graph depicts mean ± SEM (n ≥ 8 NMJs per genotype from ≥ 4 animals per genotype, one-way ANOVA, *** p < 0.001).

Figure 4. *Drosophila* Synaptogyrin mediates Tau association with synaptic vesicles *in vivo* and *in vitro*. *Drosophila* larvae express pathological mutant UAS-Tau, UAS-Tau ΔN, and/or UAS-*syngr* shRNA under control of the D42-Gal4 motor neuron promoter on a wildtype (WT) or *syngr*$^{+/-}$ background. (A) Representative confocal images of immunolabeled Tau (DAKO antibody) and SVs (CSP antibody) at *Drosophila* NMJs. White arrowheads indicate presynaptic boutons. Boutons marked with yellow arrowheads are shown enlarged in (B). Scale bars are 5 µm. (C) Plot of relative colocalization of Tau and CSP upon heterozygous loss or knockdown of Syngr in larvae expressing pathological Tau mutants. Graph depicts mean ± SEM (n = 10-28 NMJs from ≥ 6 animals per genotype, one-way ANOVA, each condition compared to Tau-only for each respective mutant genotype, *** p < 0.001). (D) Representative immunoblots detecting recombinant human Tau binding to SVs isolated from WT or *syngr* KO fly brains in the co-sedimentation assay as quantified in (E). CSP serves as loading control for SVs. Graph depicts mean ± SD (n = 4 experiments, Student's t-test, *** p < 0.001). See also Figure S3.

Figure 5. Reduction of Synaptogyrin rescues Tau-induced defects in synaptic vesicle mobility and neurotransmitter release at *Drosophila* neuromuscular junctions. (A-E) FRAP assay of SV mobility within presynaptic boutons. *Drosophila* larvae express UAS-Syt-GFP and UAS-Tau under control of the D42-Gal4 motor neuron driver on a WT or *syngr*$^{+/-}$ background. (A) Representative images of Syt-GFP signal before and after photobleaching show fluorescence recovery after photobleaching of small area (arrowhead) of Syt-GFP fluorescence in presynaptic bouton during 60 s. Control is D42 > Syt-GFP only. Scale bar is 5 µm. (B-E) Plots of Syt-GFP fluorescence recovery over time fit to a double-exponential curve. Plots depict mean ± SEM (n = 10-15 boutons from ≥ 5 animals, two-way ANOVA, *** p < 0.001, n.s. – not significant). (F-H) Electrophysiological recordings of neurotransmitter release at NMJs. (F) Plot of evoked junction potential (EJP) amplitudes in response to 10 Hz stimulation with 2 mM Ca^{2+} for 10 min in control (D42 driver only), D42 > Tau^{P301L}, Tau^{P301L} *syngr*$^{+/-}$, and *syngr*$^{+/-}$ larvae. Amplitudes are binned at 30 s intervals and normalized to the average of the first 15 s. Graph depicts mean ± SEM (n NMJ recordings indicated, 1 NMJ per animal). (G) Representative raw data traces. (H) Relative EJP amplitude at 600 s plotted as individual data points. Graph depicts mean ± SEM (one-way ANOVA, ** p < 0.01, n.s. – not significant). See also Figure S4.

Figure 6. Synaptogyrin-3 mediates Tau localization to presynaptic vesicle clusters and defects in synaptic vesicle mobility in primary hippocampal neurons from Tau transgenic mice. (A-C) Confocal imaging of Tau localization to presynaptic SV clusters. (A) Representative confocal

images of Tau^{P301S} neurons (at DIV 17) transduced with lentivirus co-expressing RFP and or Syngr3 knockdown or scrambled control shRNAs, and immunolabeled for Tau^{P301S} (hTau HT7 antibody), the SV marker Synapsin (Syn) and the dendritic marker MAP2. White arrowheads indicate presynaptic Syn puncta along axons. Scale bar is 5 µm. (B) Quantification of Tau^{P301S} localization to SVs (Pearson coefficient of Tau and Syn along axons). (C) Quantification of overall Tau^{P301S} levels (hTau intensity along axons). Graphs depict mean ± SEM (n = 85 axons from $\geq$ 24 coverslips per condition from 6 independent cultures, one-way ANOVA, *** $p < 0.001$, n.s. – not significant). (D-F) Synaptophysin-eGFP (Syph-eGFP) dispersion assay to measure SV mobility. Neurons from non-transgenic (Non Tg) littermates or Tau^{P301S} mice were transduced with lentivirus expressing Syph-eGFP only or in combination with scrambled or Syngr3 shRNA virus. (D) Representative images of Syph-eGFP fluorescence intensity during sustained 30 Hz stimulation. White arrowheads indicate presynaptic Syph-eGFP puncta (SV clusters). Scale bar is 1 µm. (E-F) Plots depicting change in Syph-eGFP fluorescence intensity in Non Tg and Tau^{P301S} neurons (E) or in Tau^{P301S} neurons co-transduced with shRNA virus (F). Neurons were imaged at rest for 30 s then stimulated at 30 Hz in a field stimulation chamber for 3 min during live imaging in 1 s intervals. The change in fluorescence was calculated for $\geq$ 20 puncta from $\geq$ 3 axons per coverslip then averaged to give n = 1 trace per coverslip. Plots depict mean ± SEM (n traces/coverslips indicated from $\geq$ 5 independent cultures, two-way ANOVA, ** $p < 0.01$, *** $p < 0.001$). See also Figure S5.

Figure 7. Reduction of Synaptogyrin-3 rescues Tau-induced defects in neurotransmitter release in primary hippocampal neurons from Tau transgenic mice. (A) Representative traces from electrophysiological recordings of autaptic hippocampal neurons in response to 10 consecutive high frequency stimulation trains (10 Hz for 10 s with 30 s rest intervals, 4 mM Ca^{2+}) by patch clamp electrophysiology. (B-C) Relative first evoked excitatory postsynaptic currents (eEPSCs) for each train plotted to train number from recordings of neurons from Tau^{P301S} mice or Non Tg littermates (B) or neurons from Tau^{P301S} mice transduced with shRNA virus (C). Plots depict mean ± SEM (n recordings indicated from $\geq$ 3 independent cultures, some error bars too small to be seen, two-way ANOVA, *** $p < 0.001$). See also Figure S6.

STAR Methods

CONTACT FOR REAGENT AND RESOURCE SHARING

Further information and requests for resources and reagents should be directed to and will be fulfilled by the Lead Contact, Patrik Verstreken (patrik.verstreken@kuleuven.vib.be).

EXPERIMENTAL MODEL AND SUBJECT DETAILS

Tau PS19 mice

All animal studies were performed under the guidelines and approval of the KU Leuven Animal Ethics Committee, which conforms to national and EU FELASA guidelines on animal welfare. Animals were housed in a conventional vivarium with a 12 h light cycle and fed standard chow and water. The generation and characterization of the Tau PS19 mouse model has been previously described (Yoshiyama et al., 2007). PS19 mice expressing human Tau^{P301S} (1N4R isoform) under control of the mouse prion promoter were obtained from JAX (Stock # 008169, strain name: B6;C3-Tg(Prnp-MAPT*P301S)PS19Vle/J). The colony was maintained by mating Tau PS19 hemizygous males to unrelated wildtype C57BL/6 females. Hemizygous Tau PS19 transgenic mice were identified by genotyping using the primers 5'-GGGGACACGTCTCCACGGCATCTCAGCAATGTCTCC–3' (forward) and 5'–TCCCCCAGCCTAGACCACGAGAAT–3' (reverse) which gives a $hTau^{P301S}$ transgene-specific PCR product at 350 bp. An internal control primer pair (forward 5'–CAAATGTTGCTTGTCTGGTG–3', reverse 5'–GTCAGTCGAGTGCACAGTTT–3'), which gives a PCR product at 170 bp, was used as a positive control. DNA from embryonic tails was prepared and processed for genotyping using the KAPA Mouse Genotyping HotStart Kit (KAPA Biosystems) according to manufacturer's instructions.

Primary mouse hippocampal neurons

For primary neuronal cultures, hemizygous Tau PS19 males on a C57BL/6 background were mated with wildtype C57BL/6 female mice from an unrelated colony. Embryos were harvested on day E17.5, and brains isolated and dissected in room-temperature Hank's balanced salt solution (HBSS) + 10 mM HEPES (pH 7.4) to obtain the hippocampi. Hippocampal pieces were incubated with 0.25% trypsin and 0.1 mg/mL DNase in HBSS for 15 min at 37 °C, followed by three washes in HBSS before resuspension in prewarmed MEM containing 10% (v/v) horse serum, 33 mM D-glucose, and 1X Pen-Strep (Invitrogen). Hippocampal pieces were gently triturated with glass Pasteur pipettes of decreasing size to obtain a single-cell suspension. Neurons were plated at a density of ~55,000 cells per 18 mm glass coverslip (nitric acid-washed and coated with 0.1 mg/mL poly-lysine and 1 µg/mL laminin). 2-4 h after plating, the medium was replaced with NB-B27 medium (Neurobasal medium + 1x B27 supplement, 0.5 mM Glutamax, 0.2x Pen-Strep, Invitrogen). Neurons were kept in a 37 °C incubator with 5% CO_2. 1/3rd of the medium was

replaced with fresh medium every 7 days. Neurons from hippocampi of each independent embryo were individually cultured and genotyped (embryonic tails collected during dissection) to determine Tau PS19 or Non Tg littermate. For establishing primary cultures, embryo gender was not analyzed. For functional assays, neurons from Non Tg littermates were used as controls in comparison to neurons hemizygous for the Tau^{P301S} transgene.

Fly stocks

Drosophila melanogaster fly stocks were handled using standard protocols. All experimental crosses involving the UAS/Gal4 bipartite expression system were kept at 25 °C to induce transgene expression. Experiments at the neuromuscular junction (NMJ) utilized the motorneuron-specific driver D42-Gal4. We previously described the generation and characterization of wildtype or FTDP-17 clinical mutant 0N4R (383 aa) Tau variants (P301L, V337M, R406W) or N-terminally truncated ΔN_Tau mutants into the 68A4 locus on chromosome III (Zhou et al., 2017). All transgenic flies were kept on the w^{1118} strain background. The D42-Gal4 driver was recombined together with UAS-Tau genes onto chromosome III and, where necessary, additionally combined with the *syngr*^{1} loss-of-function allele on chromosome II (to give heterozygous *syngr*$^{+/-}$) or UAS-Synaptotagmin-eGFP on chromosome II. *Syngr* KO flies (*syngr*^{1} loss-of-function allele, w1118 background) were previously generated by and gifted from the J. Troy Littleton lab (R. J. Stevens et al., 2012). Control crosses were to wildtype w1118 strain for consistency of the genetic background. The UAS-Synaptotagmin-eGFP stock was obtained from the Bloomington Stock Center (stock 6925) and the UAS-*syngr* shRNA stock is HMS01724 from the *Drosophila* Transgenic RNAi project (TRiP, Bloomington stock 38274). Other loss-of-function/knockdown alleles and stocks used in the SV interactor genetic screen include *syt*^{AD4} (DiAntonio et al., 1993), *synj*^{2} (Verstreken et al., 2003), UAS-*rph* shRNA (TRiP JF01970, Bloomington stock 25950), *shi*$^{12\text{-}12B}$ (Kasprowicz et al., 2014), and *pnut*^{XP} (Bloomington stock 5687).

Human subjects

Post-mortem brain tissue (posterior hippocampal samples) was obtained from the Edinburgh Brain and Tissue Bank at the University of Edinburgh. The use of human tissue samples conformed to national and institutional ethics guidelines and was approved by the Edinburgh MRC Brain and Tissue Bank Ethics Committee and the Academic and Clinical Central Office for Research and Development medical research ethics committee (approval 15-HV-016). Case information for all patient samples used in this study can be found in Table S1.

METHOD DETAILS

Isolation of synaptic vesicles

Isolation of crude synaptic vesicles (LP2 fraction) from mammalian brain or *Drosophila* adult fly brain was performed based on protocols (Ahmed et al., 2013) and (Depner et al., 2014), respectively, with modifications. For detailed fractionation centrifugation speeds and times see the respective schematics presented in Figures S1 and S2. All steps of fractionation experiments were carried out on ice or at 4 °C. Aliquots of pellets were saved at various steps during fractionation and were lysed in RIPA buffer (150 mM NaCl, 1.0% IGEPAL CA-630/NP-40, 0.5% sodium deoxycholate, 0.1% SDS, 50 mM Tris, pH 8.0, Sigma) containing protease and phosphatase inhibitors and stored at -80 °C until analysis. Briefly, frozen (human) or fresh (mouse) brain tissue was chopped into 5 mm^2 cubes, and homogenized in sucrose buffer (320 mM sucrose, 4 mM HEPES pH 7.4, 1X Complete protease inhibitor cocktail (Roche), 1X PhosStop phosphatase inhibitor cocktail (Roche) at a volume of 9 mL per 1 g human brain sample or 3 mL per six-week-old mouse brain (C57BL/6 strain). For fly brains, 5 mL of sieved and collected fly heads were ground in a liquid nitrogen-cooled mortar with a pestle into fine powder and resuspended in 15 mL sucrose buffer per 5 mL adult fly heads. Homogenization was performed using 10 strokes at 600 pm (human and mouse brain) or 900 rpm (fly brain) in a Teflon glass homogenizer. Following pelleting of cell debris and nuclei, synaptosomes were isolated and washed once by resuspension in 10 mL sucrose buffer and re-pelleted. Synaptosomes were hypotonically lysed by resuspension of the synaptosome pellet in 10 volumes of HEPES-buffered water (5 mM HEPES pH 7.4, 1X Protease inhibitor cocktail, 1X Phosphatase inhibitor cocktail and Pepstatin A (Roche, fly samples) and incubated for 30 min at 4 °C with rotation. For fly brains, the osmotic shock suspension was homogenized using 3 strokes at 2000 rpm. Following osmotic shock, a 25,000 x g centrifugation step removed mitochondria and large synaptic membrane debris; finally, synaptic vesicles were collected from the supernatant by centrifugation at 165,000 x g for 2 h. The resulting crude synaptic vesicle pellet (LP2/SV) was resuspended in SV resuspension buffer (5 mM HEPES pH 7.4, 300 mM glycine) and frozen in aliquots at -80 °C. Vesicles were quantified according to protein content using the Bradford Quick Start reagent (Bio-Rad). The purity of the LP2/SV fraction was verified by immunoblotting 20 µg of protein from fractionation pellets (lysed in RIPA buffer) or 20 µg vesicle suspension for synaptic vesicle markers or contaminates.

SDS-PAGE and immunoblotting

For denaturation of protein samples, 4X lithium dodecyl sulfate (LDS, Invitrogen) was added to samples to a final concentration of 1X supplemented with 1% β-mercaptoethanol and denatured for 10 min at 70-80 °C. Protein samples were separated on NuPAGE 10%, 12% or 4-12% Bis-Tris mini polyacrylamide gels in MOPS buffer (Invitrogen), or 4-15% Bis-Tris Criterion TGX midi protein gels in Tris-Glycine-SDS buffer (Bio-Rad). For colloidal coomassie staining, gels were stained with PageBlue staining solution (Thermo Fisher) according to manufacturer's instructions. For immunoblotting, protein gels were transferred to nitrocellulose membranes using the TransBlot

Turbo transfer system (Bio-Rad). Membranes were blocked in TBS-T (1X Tris-Buffered Saline solution + 0.05% Tween-20) with 5% (w/v) milk powder for 30-60 min at room temperature. Primary antibodies were diluted in blocking buffer (see table below) and incubated with membranes for 1-2 h at room temperature or overnight at 4 °C, followed by 4 x 10 min washing in TBS-T. Secondary HRP-conjugated antibodies (Jackson Immunoresearch) were diluted 1:10,000 in blocking buffer and incubated with membranes for 1 h at room temperature, then washed for 6 x 10 min in TBS-T. Immunoblots were developed using the Western Lightning Plus enhanced chemiluminescence kit (Perkin Elmer) and imaged on a Fuji Film imaging system. Densitometry analysis was performed using Image Studio Lite.

Purification of recombinant human Tau

We previously described the purification of soluble recombinant human Tau from bacteria (Zhou et al., 2017). The cDNA sequences encoding human full-length Tau (0N4R isoform, 383 aa) or ΔN_Tau (aa 113-383) were cloned behind a N-terminal GST tag and PreScission Protease cleavage sequence in the pGEX-6P-1 plasmid and was followed by a C-terminal 8x-His tag (inserted into the reverse amplification primer). Sequence-verified plasmids were transformed into Rosetta bacteria (Novagen) and maintained in medium containing ampicillin and chloramphenicol. Overnight pre-cultures were diluted 1:10 into LB medium, incubated for 2 h at 37 °C to exponential phase, and then expression was induced by addition of IPTG to a final concentration of 0.4 mM. Expression was carried out for 2 h at 37 °C, followed by pelleting of cells (5,000 x g for 15 min); cell pellets were stored at -80 °C until use. For purification, all steps were carried out on ice or at 4 °C. A 50 mL cell pellet was resuspended in 1.5 mL lysis buffer (1X PBS supplemented with 1X protease inhibitor cocktail, Lysozyme, Benzonase, 1% Triton-X-100, and 10% glycerol) and incubated for 30 min at 4 °C with mixing. Lysates were clarified by centrifugation at 16,000 x g for 20 min, then incubated with 150 µL washed Glutathione Sepharose 4B (GE Healthcare) for 2 h at 4 °C. Glutathione Sepharose beads were washed 3 times with PBS supplemented with 250 mM NaCl, and 2 times with PreScission Protease cleavage buffer (20 mM Tris-HCl pH 7.0, 50 mM NaCl, 0.5 mM EDTA, 1 mM DTT, 0.01% Tween-20). Beads were incubated overnight at 4 °C with GST-tagged PreScission Protease (GE Healthcare) in cleavage buffer to remove the N-terminal GST tag and liberate Tau from the Sepharose beads. The next morning, the supernatant was incubated for 1 h with 75 µL fresh, washed Glutathione Sepharose to remove any unbound protease or uncleaved Tau. Cleaved Tau-8xHis was then purified against the C-terminal His tag by incubation with 50 uL Ni-NTA resin (Bio-Rad) for 45 min, then washed 3x in His wash buffer (50 mM NaH_2PO_4 pH 8.0, 300 mM NaCl, 20 mM imidazole), and eluted by incubation with His elution buffer for 15 min (same buffer with 250 mM imidazole). Purified Tau was concentrated using an Amicon Centrifugal Filter unit with 10 kDa molecular weight cut-off (Millipore) and quantified using the Bradford Quick Start reagent. Using this method, purification of one 50 mL

cell pellet yields approximately 8 µg of soluble Tau with >95% purity. For all experiments, Tau was always purified freshly and used immediately upon finishing purification.

In vitro synaptic vesicle binding assays

The ability of purified recombinant Tau to bind isolated synaptic vesicles *in vitro* was assessed using a vesicle sedimentation assay (Piccoli et al., 2014; Zhou et al., 2017). In this assay, 500 ng of freshly purified Tau-8xHis was incubated together with 20 µg (according to protein) isolated synaptic vesicles in 100 µL SV binding buffer (4 mM HEPES pH 7.4, 5 mM Tris-HCl pH 7.4, 220 mM glycine, 30 mM NaCl, 1X protease inhibitor cocktail) for 2 h at 4 °C with rotation. The 100 µL binding reaction was then diluted into 600 µL binding buffer to prevent tubes from breaking during centrifugation. Vesicles were pelleted by ultracentrifugation at 165,000 x g for 1 h, and the pellet was resuspended and denatured in 1X LDS sample buffer. The presence of Tau co-sedimenting together with synaptic vesicles in the pellet fraction (detected by immunoblotting of the vesicle pellet with anti-His antibody) indicates binding.

Limited proteolysis of synaptic vesicles was carried out by incubating 75 µg synaptic vesicles together with 50 µL sepharose-coupled TPCK-treated trypsin (Thermo Fisher) for 3 h at 37 °C. After 3 h, proteolysis was halted by the addition of 1X protease inhibitor cocktail, 1 mM PMSF, and 0.5 mg/mL soybean trypsin inhibitor (Sigma) and the sepharose-conjugated trypsin was removed by centrifugation at 3,000 x g to remove the sepharose slurry. As a control, untreated vesicles were incubated at 37 °C for 3 h but in the absence of trypsin.

To remove peripheral synaptic vesicle-associated proteins, vesicles were stripped with carbonate (Brose et al., 1995). Isolated synaptic vesicles were diluted in buffer containing 100 mM Na_2CO_3 pH 11 and 1X protease inhibitors and incubated at 4 °C for 30 min. Vesicles were pelleted by ultracentrifugation at 165,000 x g for 1 h then resuspended in neutral buffer (5 mM HEPES pH 7.4, 300 mM glycine). As a control, unstripped vesicles were handled the same except diluted in neutral buffer instead of carbonate buffer. Equal volumes of untreated or carbonate-stripped vesicles were introduced into the binding reaction.

Liposome flotation assay

The liposome flotation assay is based on a protocol previously described (Bigay et al., 2005). To generate small protein-free liposomes 0.25 mg of bovine brain Folch-fraction lipid extract (Avanti Lipids) was dried under a nitrogen stream and desiccated overnight in a vacuum chamber. Liposomes of 30-60 nm diameter were generated by adding 250 µL warmed SV binding buffer to the lipid film and sonicating for 5 min in a 37 °C bath. Electron microscopy verified uniform 30-60 nm diameter of liposomes. 64 µg of liposomes was mixed together with 1.5 µg freshly purified Tau in 150 µL SV binding buffer and incubated together for 1 h at 4 °C. After 1 h, the density of the binding reaction was adjusted to 30% (w/v) sucrose by addition of 100 µL of a 75% sucrose

solution. The 250 µL binding reaction in 30% sucrose was overlaid with a middle 200 µL layer of 25% sucrose and a top layer of 50 µL SV buffer (no sucrose). The gradient was centrifuged at 240,000 x g for 1 h at 4 °C, and then 30 µL fractions from the bottom, middle, or top layers were collected, denatured with LDS and immunoblotted for Tau with anti-His antibodies. Due to their density, liposomes rise to the top sucrose-free fraction during centrifugation, together with any proteins bound to them. Thus, immunoblotting for protein present in the top fraction indicates binding to liposomes.

Tau co-IP and mass spectrometry

Synaptic vesicles isolated from mouse brains (LP2/SV fraction) were lysed in 2% Triton-X-100 in SV resuspension buffer (5 mM HEPES pH 7.4, 300 mM glycine) for 1 h at 4 °C, followed by clearing of membrane debris and intact vesicles by centrifugation at 165,000 x g for 1 h. The SV lysate was diluted in SV binding buffer to a final concentration of 0.6% Triton-X-100 and supplemented with fresh protease inhibitors and NaCl to a final concentration of 100 mM. For co-immunoprecipitation, 2 µg of purified Tau^{FL}-8xHis or $Tau^{\Delta N}$-8xHis was bound to 25 µL of washed Protein G Dynabeads (Invitrogen) using 1 µg mouse anti-His IgG antibody (Thermo Fisher, clone 4A12E4) for 2 h at 4 °C. Beads were washed twice then incubated with SV lysate (330 µg protein per reaction, 0.6% Triton-X-100, 100 mM NaCl) in SV buffer with 1% BSA and fresh protease inhibitors overnight at 4 °C with rotation. As a negative control, we incubated SV lysate together with Dynabeads containing only the anti-His IgG antibody. After the overnight incubation, beads were washed three times with SV buffer + 0.6% Triton-X-100 and three times with SV buffer to remove detergents. Samples were immediately processed for mass spectrometry.

Intact Tau-protein complexes were processed using on-bead digestion by overnight incubation with 0.2 mg/mL trypsin in 50 mM ammonium bicarbonate buffer at 37 °C. The resulting peptide mixture was dried in a SpeedVac, and the peptide pellet was resuspended in loading solvent (2% acetonitrile, 0.1% trifluoroacetic acid). $1/10^{th}$ of each sample was run in triplicate by LC-MS/MS by 30 min separation on a 2-50% gradient of solvent (80% acetonitrile, 19.9% water and 0.1% formic acid) coupled to a LTQ-Orbitrap XL mass spectrometer. Peptide spectra were searched with Mascot Daemon software against a *Mus musculus* protein database to identify proteins. The unfiltered mass spectrometry dataset is shown in Table S2. Identified proteins were cross-referenced against comprehensive lists of synaptic vesicle proteins (Burré et al., 2006; Takamori et al., 2006) and were classified as transmembrane SV proteins, peripheral SV proteins, or non-SV proteins (likely contaminates). A filtered list of identified SV-specific proteins absent in the negative control is shown in Figure 1I. Mass spectrometry experiments were performed at the VIB Proteomics Core (University of Ghent, Belgium).

Immunofluorescence in *Drosophila* larvae

For immunofluorescence at *Drosophila* larval NMJs, wandering third-instar larvae were dissected in freshly prepared HL3 buffer (110 mM NaCl, 5 mM KCl, 10 mM $NaHCO_3$, 5 mM HEPES, 30 mM sucrose, 5 mM trehalose, pH 7.4) on Sylgard-coated plates then fixed in HL3 + 3.7% formaldehyde for 20 min at room temperature. Larvae were gently dissected in calcium-free, low potassium (5 mM KCl) HL3 buffer to avoid stimulation and therefore maintain a tight peripheral distribution of SVs close to the presynaptic membrane. Larval filets were transferred to microcentrifuge tubes, washed with PBS and permeabilized with PBS + 0.4% Triton-X-100 for 1 h at room temperature then blocked for 1 h in blocking buffer (PBS + 1% BSA + 0.4% Triton-X-100). Primary antibody incubation was performed overnight (1:1000 dilution, see antibody table) in blocking buffer. After overnight incubation, larvae were washed 3 x 20 min (PBS + 0.4% Triton-X-100) then incubated for 2 h with Alexa-Fluor-488 or -555 antibodies (Invitrogen) diluted 1:1000 in blocking buffer, followed again by washing 3 x 20 min. Larvae were mounted on glass slides using VectaShield Antifade mounting medium (Vector Laboratories). Images of NMJs at segments A2/A3 of larval muscles 12/13 were acquired with a Nikon A1R confocal laser scanning microscope by acquiring Z-stacks through the entire NMJ in 0.2 µm depth intervals with a 1.0 Airy unit pinhole opening. All images of NMJs shown are maximum projections of Z-stacks.

FRAP assay of synaptic vesicle mobility

The use of a fluorescence recovery after photobleaching (FRAP) assay to assess synaptic vesicle mobility has been described previously (Seabrooke et al., 2010; Zhou et al., 2017). Flies expressing UAS-Synaptotagmin-GFP and UAS-Tau under control of the D42-Gal4 promoter were crossed with WT (w^{1118} strain) or *syngr* KO flies to give a *syngr* +/- background. Third-instar larvae were dissected in fresh HL3 buffer and pinned down to Sylgard-coated plates. Synaptotagmin-GFP fluorescence was visualized on a Nikon A1R confocal laser microscope with a 60x 1.0 N.A. water immersion objection immersed in HL3 buffer. Images were acquired at 1.12 µs/px, pinhole 1 airy unit, resolution 512 x 512 px using the 488 nm laser line and appropriate filters for GFP fluorescence. All recordings were made from boutons at segments A2/A3 of muscles 12/13. Boutons were selected to ensure flat geometry and similar fluorescence volume and intensity both within the photobleached spot and in the entire bouton. Following acquisition of a pre-bleach baseline, a small spot (24 x 30 px) on the periphery of the bouton was photobleached using 95% laser power of both 405 nm and 488 nm laser lines (9 iterations). Imaging at normal acquisition settings was continued at 1 s intervals for 60 s.

Electrophysiology at *Drosophila* larval NMJs

For electrophysiology, flies expressing D42 > UAS-Tau^{P301L} (recombined on chromosome III) were crossed to WT or *syngr* KO flies to give a $syngr^{+/-}$ background. Larvae were dissected in HL3 buffer on sylgard-coated plates. Stimulation and recordings were performed in room-temperature HL3 buffer supplemented with 0.5-2 mM $CaCl_2$ as indicated in the figure legend. Axons innervating

NMJs at segments A2/A3 of larval muscles at 12/13 were cut and used for intracellular voltage recordings using sharp electrodes (~20 MΩ resistance, 2X stimulation threshold). NMJ miniature or evoked excitatory junction potentials were recorded with an Axoclamp 900A amplifier and digitized with a Digi-data 1440A device, and recorded in pClamp software (version 10.2, Molecular Devices). For 10 Hz stimulation, EJP amplitudes were binned every 30 s and normalized to the amplitude measured in response to the first 15 stimuli.

Viruses and transduction of primary neurons

Scramble and *syngr3* knockdown vectors: Transfer plasmids encoding RFP (CMV promoter) and scramble or anti-mouse/rat *syngr3* shRNAs (U6 promoter) were produced in the pRFP-CB-shLenti plasmid by Origene. The shSyngr3 A targeting sequence is 5'-GTTCGTAGGCTTCTGTTTCCTCACCAATC-3' and the shSyngr3 B targeting sequence is 5'-GAGCCTGCCGCTTCGGCGTCGTACTAGGT-3'. The shScramble sequence is 5'-GCACTACCAGAGCTAACTCAGATAGTACT-3'. The loop sequence is 5'-TCAAGAG-3'.

Synaptophysin-eGFP vector: The cDNA sequence encoding rat Synaptophysin (307 aa) was cloned upstream of a C-terminal eGFP fusion tag (238 aa) in a second-generation lentiviral transfer plasmid under control of the rat 1.1 kb Synapsin-1 promoter fragment.

Transfer plasmids, the psPAX2 packaging plasmid, and the pMD2.G envelope plasmid (Addgene) were propagated in TOP10 cells (Invitrogen) and plasmid DNA was purified for transfection using a Plasmid Plus Midi Kit (Qiagen). 1.3 x 10^7 HEK 293T cells (50-70% confluency) in a T175 flask were transfected with 1 µg pMD2.G, 9 µg psPAX2, and 10 µg transfer plasmid with Lipofectamine-2000 (Invitrogen) according to manufacturer's instructions in DMEM + 2% fetal bovine serum (FBS). 6 h after the start of transfection, the medium was replaced with 15 mL fresh DMEM + 10% FBS. Conditioned medium containing lentiviral particles was collected 48 h after the end of transduction, was passed through a 0.2 µm filter and concentrated using a Amicon Centrifugal Filter Unit with a 100 kDa molecular weight cut-off to a final volume of 1 mL, then was aliquoted, snap-frozen and stored at -80 °C until use. The viral titer was empirically tested; in general, 10-20 µL of concentrated lentivirus-containing medium (15 mL from one T175 flask concentrated to 1 mL) was used to transduce ~55,000 neurons on a 18 mm coverslip in a 12-well plate, which routinely gave > 95% transduction efficiency.

Primary hippocampal neurons were transduced on DIV4 or DIV5. Half of the culture medium was removed and moved to a new plate, to which another half of fresh NB-B27 medium was added. 10-20 µL of each lentivirus was added to each coverslip and left for 6 h to infect neurons. After 6 h, the lentivirus-containing medium was completely removed and was replaced with the half-conditioned/half-fresh NB-B27 mix. Medium was not changed again for 7 days following transduction.

Immunofluorescence of hippocampal neurons

DIV 17 neurons were washed once with PBS (with $MgCl_2$ and $CaCl_2$) and fixed (4% paraformaldehyde + 4% sucrose in PBS) for 25 min at room temperature. Neurons were permeabilized and blocked by incubation with 5% goat serum, 2% BSA, 0.3% Triton-X-100 in PBS for 1 h at room temperature. Coverslips were incubated with primary antibody (see table for dilutions) overnight at 4 °C in PBS with 2% goat serum, 2% BSA and 0.1% Triton-X-100. The next day coverslips were washed 3 x 5 min in PBS, then incubated with secondary Pacific Blue, Alexa-Fluor-488, -555 or -647 antibodies (Invitrogen) diluted 1:500 in PBS with 2% goat serum, 2% BSA and 0.1% Triton-X-100 for 2 h at room temperature. Following 3 x 5 min washes in PBS, coverslips were mounted onto glass slides with VectaShield Antifade mounting medium (Vector Laboratories). Images were acquired on a Nikon A1R confocal microscope with 1 Airy unit pinhole opening. All images of primary neurons shown are single optical sections (0.2 µm depth).

Synaptic vesicle dispersion assay

The vesicle dispersion assay to measure synaptic vesicle mobility in primary hippocampal neurons is based on a protocol previously described (L. Wang et al., 2014). Coverslips containing DIV17 hippocampal neurons transduced on DIV4-5 with lentivirus expressing Synaptophysin-eGFP and, where indicated, lentivirus encoding scramble or anti-*syngr3* shRNAs, were transferred out of their medium and bathed for 5 min in recording buffer (25 mM HEPES pH 7.4, 119 mM NaCl, 2.5 mM KCl, 2 mM $CaCl_2$, 2 mM $MgCl_2$, 30 mM glucose) supplemented with 50 µM D-APV (Abcam) and 10 µM CNQX (Sigma) to halt ongoing network activity. Coverslips were transferred into a RC-49MFSH field stimulation chamber (Warner Instruments) and the coverslip was sealed around the edges with oil. Platinum wire electrodes on either side of the recording chamber were connected to the stimulus isolator unit. Room-temperature recording buffer was added to cover the electrodes, and a 60X 1.0 N.A. water-immersion objective was dipped into the chamber. Live imaging was performed on an upright Nikon A1R confocal microscope, using a pinhole opening of 5 Airy units in 1 s intervals using 0.5-1.0% laser power in the 488 nm laser line with acquisitions in 1 s intervals. Fluorescence was recorded for 30 s to ensure no photobleaching or loss of focus before stimulation began. From 30 s onwards, neurons were stimulated for 180 s by delivering 1 ms pulses at 33.3 ms intervals (30 Hz) using a A310 Accupulser (World Precision Instruments) connected to a A365 Stimulus Isolator (World Precision Instruments) set to 50 mA and unipolar mode. All stimulation and acquisition was performed at room-temperature.

Electrophysiology of hippocampal neurons

The establishment of autaptic neuronal cultures has been previously described (Bekkers and C. F. Stevens, 1991; Burgalossi et al., 2012). Glass coverslips were coated with agarose, dried and subsequently grid-stamped with a mixture of poly-lysine and rat-tail collagen. Primary astrocytes

dissociated from cortices of P0 NMRI mouse pups (Charles River) were cultivated to 60-70% confluence in a flask (~1 week) containing DMEM + 10% FBS. For island preparation, 25,000 astrocytes were plated per 30 mm glass coverslip in 6-well plates and allowed to form micro-dot islands in DMEM + 10% FBS for 3-5 days. Medium was then exchanged for modified NB-B27 medium (Neurobasal medium + 1x B27 supplement, 0.5 mM Glutamax, 12 mM D-glucose, 25 µm β-mercaptoethanol, 0.2x Pen-Strep, Invitrogen), and 2,500 hippocampal neurons were plated directly onto islands. Where indicated, neurons were transduced with lentivirus on DIV5 for 6 hours, followed by a single one-half volume medium change.

Whole-cell voltage clamp recordings were performed on DIV17-19 isolated neurons. The intracellular pipette solution contained 136 mM KCl, 18 mM HEPES, 4 mM Na-ATP, 4.6 mM $MgCl_2$, 4 mM K_2-ATP, 15 mM Creatine Phosphate, 1 mM EGTA and 50 U/mL Phospocreatine Kinase (300 mOsm, pH 7.30). The extracellular solution used during recordings contained 140 mM NaCl, 2.4 mM KCl, 4 mM $CaCl_2$, 4 mM $MgCl_2$, 10 mM HEPES, 10 mM glucose (300 mOsm, pH 7.30). Neurons were whole-cell voltage clamped at 70 mV using a double EPC-10 amplifier (HEKA Elektronik, Lambrecht/Pfalz, Germany) under control of Patchmaster v2 x 32 software (HEKA Elektronik). Currents were recorded at 20 Hz and low-pass filtered at 3 kHz when stored. Pipettes were pulled using a Sutter P-1000 and resistance ranged from 3 to 5 MΩ. The series resistance was compensated to 75-85%. Cells with series resistances above 15 MΩ were excluded for analysis. Spontaneous glutamatergic release was (sEPSC) was recorded at -70 mV. Evoked release was induced using brief depolarization of the cell soma (from 70 to 0 mV for 1 ms) to initiate action potential-dependent glutamatergic release (eEPSCs). All recordings were performed at room temperature.

QUANTIFICATION AND STATISTICAL ANALYSIS

Localization studies at NMJs

To quantify the association between Tau and CSP-labeled synaptic vesicles *in vivo* at *Drosophila* NMJs, we used the “Colocalisation Test” plug-in in ImageJ software. Each bouton at an NMJ was individually encircled as an ROI, and the Z-position was selected where CSP was the widest/most peripheral around the bouton. The “Colocalisation Test” plug-in (Image J) was run to measure the overlap between the Tau (DAKO antibody) and CSP channels using 75 iterations and measuring only on the individual Z-section. The R(obs) value was taken as the Pearson’s colocalization coefficient. To account for the high baseline Pearson coefficient value due to the large area of the bouton occupied by CSP-labeled synaptic vesicles, we also calculated the Pearson coefficient between CSP and a Fay-randomized (random noise) image generated by the colocalization test plug-in to simulate the baseline colocalization value between CSP and a completely diffuse signal. This value was subtracted from the measured CSP-Tau Pearson

coefficient to calculate the relative colocalization value (control set to 1). The same analysis was performed for every bouton at a given NMJ and averaged to give n = 1 data point per NMJ.

FRAP analysis of SV mobility at NMJs

The intensity of the bleached spot, plotted as percent of initial fluorescence, was normalized to a non-bleached reference bouton and measured using Nikon analysis software (NIS-Elements AR 4.5), and the trace was fit to a double-exponential curve in GraphPad Prism 7 software. FRAP traces from 2-4 boutons were acquired per larvae.

Localization studies in hippocampal neurons

The quantification of the presynaptic localization of Tau in hippocampal neurons was measured as the Pearson colocalization coefficient between $hTau^{P301S}$ (HT7 antibody) and the synaptic vesicle marker Synapsin. Entire axon segments of approximately 20 µm were selected as ROIs. Distal axon segments (at least 60 µm away from cell body) were randomly chosen using Synapsin and RFP channels in an unbiased way. The "Colocalisation Test" plug-in in ImageJ was then run on acquired images to measure the overlap between the two channels using 75 iterations and Fay randomization. The R(obs) value was taken as the Pearson's coefficient.

Quantification of $hTau^{P301S}$ levels (HT7 antibody) in axons (using same images as for presynaptic localization) was performed in ImageJ by measuring the fluorescence integrated density along axon segments (approximately 20 µm) selected as ROIs. Quantification of Syaptogyrin-3 levels were performed by measuring Synaptogyrin-3 integrated density at Synapsin-labeled presynaptic puncta. The relative intensity of 5-10 puncta per axon/cell was normalized to the Synapsin signal and then averaged to give n = 1 data point per cell. Quantification of synapse size was performed by quantifying the area of Synapsin puncta in ImageJ. Quantification of synapse number was manually counted as a function of axon segment length.

Synaptic vesicle dispersion assay

For each recording, the change in Synaptophysin-GFP puncta fluorescence intensity (t_0 was set to 100%) was quantified from 20-40 synapses (all distinct Syph-eGFP puncta in view for each coverslip were selected as individual ROIs using Nikon software) from 2-5 axons in view and averaged to give n = 1 averaged trace per coverslip.

Statistics

All statistical analyses were performed with GraphPad Prism 7.0 software. Where quantifications are shown, the graph representation and error bars are defined in each legend, together with the definition of n and which statistical test was performed. Error bars either depict standard deviation (SD) or standard error of the mean (SEM), as indicated in the figure legend. In all

instances, statistical significance was defined as follows: n.s. - not significant ($p > 0.05$), * $p < 0.05$, ** $p < 0.01$, *** $p < 0.001$. For multiple comparisons using one-way ANOVA, Dunnett's multiple comparisons test was used to compare each condition to a single control group. For two-way ANOVA, Sidak's multiple comparisons test was used to test genotype as source of variance. No outlier analysis was performed or data points excluded.

KEY RESOURCES TABLE

REAGENT or RESOURCE	SOURCE	IDENTIFIER
Antibodies		
anti-Actin mouse	DSHB	Cat#: JLA20; RRID:AB_528068
anti-ATP synthase mouse	Abcam	Cat#: ab14730; RRID:AB_301438
anti-*Drosophila* Cysteine String Protein (CSP) mouse	DSHB	Cat#: DCSP-2; RRID:AB_528183
anti-*Drosophila* Discs-large (Dlg) mouse	DSHB	Cat#: 4F3; RRID:AB_528203
anti-*Drosophila* Synaptogyrin (Syngr) rabbit	Stevens et al., 2012	N/A
anti-GAPDH mouse	EMD Millipore	Cat#: MAB374; RRID:AB_2107445
anti-His Tag mouse	Thermo Fisher	Cat#: 37-2900; RRID:AB_2533309
anti-Human Tau “hTau” (HT7) mouse	Thermo Fisher	Cat#: MN1000; RRID:AB_223454
anti-MAP2 chicken	Abcam	Cat#: ab5392; RRID:AB_2138153
anti-Munc18-1 (Munc18) rabbit	Cell Signaling	Cat#: 13414; RRID:AB_10891779
anti-phospho-Tau pSer202/pThr205 (AT8)	Thermo Fisher	Cat#: MN1020; RRID:AB_223647
anti-phospho-Tau pSer396/pSer404 (PHF-1)	Laboratory of Peter Davies	RRID:AB_2315150
anti-PSD-95 rabbit	Cell Signaling	Cat#: 3450T; RRID:AB_2292883
anti-Synapsin-1 (Syn) rabbit	EMD Millipore	Cat#: AB1543P; RRID:AB_90757
anti-Synaptic vesicle glycoprotein 2A (SV2) mouse	DSHB	Cat#: SV2; RRID:AB_2315385
anti-Synaptobrevin-2 / VAMP2 (Syb) mouse	Synaptic Systems	Cat#: 104 211; RRID:AB_887811
anti-Synaptogyrin-3 (Syngr3) mouse	Santa Cruz Biotechnology	Cat#: sc-271046; RRID:AB_10611955
anti-Synaptogyrin-3 (Syngr3) rabbit	Novus Biologicals	Cat#: NBP2-30475
anti-Synaptophysin-1 (Syph) mouse	Synaptic Systems	Cat#: 101 011; RRID:AB_887824
anti-Synaptotagmin-1 (Syt) cytoplasmic epitope mouse	DSHB	Cat#: asv 48; RRID:AB_2199314
anti-Synaptotagmin-1 (Syt) vesicular epitope rabbit	Synaptic Systems	Cat#: 105 102; RRID:AB_887835
anti-Total Tau (DAKO)	DAKO	Cat#: A0024; RRID:AB_10013724
anti-VGlut1 guinea pig	EMD Millipore	Cat#: AB5905; RRID:AB_2301751
Bacterial and Virus Strains		
Lentivirus CMV::RFP, U6::shRNA scramble	This paper	N/A
Lentivirus CMV::RFP, U6::shRNA anti-Syngr3 A	This paper	N/A
Lentivirus CMV::RFP, U6::shRNA anti-Syngr3 B	This paper	N/A

Lentivirus Synapsin::Synaptophysin-eGFP	This paper	N/A
Biological Samples		
Hippocampal tissue samples from human brain	Edinburgh Brain and Tissue Bank	http://www.ed.ac.uk/clinical-brain-sciences/research/edinburgh-brain-and-tissue-bank
Chemicals, Peptides, and Recombinant Proteins		
Recombinant human Tau protein (0N4R isoform)	(Zhou et al., 2017)	N/A
PreScission protease	GE Healthcare	Cat#: 27084301
Dynabeads protein G for immunoprecipitation	Thermo Fisher	Cat#: 10003D
D-APV	Abcam	Cat#: ab120003
CNQX	Sigma	Cat#: C127
Experimental Models: Organisms/Strains		
Mouse: C57BL/6J	JAX	Cat#: 000664
Mouse: "Tau PS19" B6;C3-Tg(Prnp-MAPT*P301S)PS19Vle/J	JAX	Cat#: 008169
D. melanogaster: UAS-hTau P301L, V337M, or R406W (0N4R isoform, attP2/68A4 insertion site)	(Zhou et al., 2017)	N/A
D. melanogaster: UAS-Synaptotagmin-GFP	Bloomington Stock Center	Cat#: 6925; RRID:BDSC_6925
D. melanogaster: UAS-syngr shRNA (TRiP.HMS01724)	Bloomington Stock Center	Cat#: 38274; RRID:BDSC_38274
D. melanogaster: *syngr*^{1} knock-out	(Stevens et al., 2012)	N/A
Oligonucleotides		
shRNA targeting sequence: scramble: GCACTACCAGAGCTAACTCAGATAGTACT	This paper	N/A
shRNA targeting sequence: mouse Syngr3 A: GTTCGTAGGCTTCTGTTTCCTCACCAATC	This paper	N/A
shRNA targeting sequence: mouse Syngr3 B: GAGCCTGCCGCTTCGGCGTCGTACTAGGT	This paper	N/A
Recombinant DNA		
Plasmid: pGEX_GST-Prescission-Tau-8x-His	(Zhou et al., 2017)	N/A
Plasmid: pRFP-CB-shLenti	Origene	Cat#: TR30032
Software and Algorithms		
NIS-Elements	Nikon	http://www.nikoninstruments.com

Graphpad Prism 7.0	GraphPad	http://www.graphpad.com
Image Studio Lite	LI-COR Biosciences	http://www.licor.com
ImageJ	NIH	http://imagej.nih.gov/ij/

Figure 1

Click here to download Figure Fig 1.tif

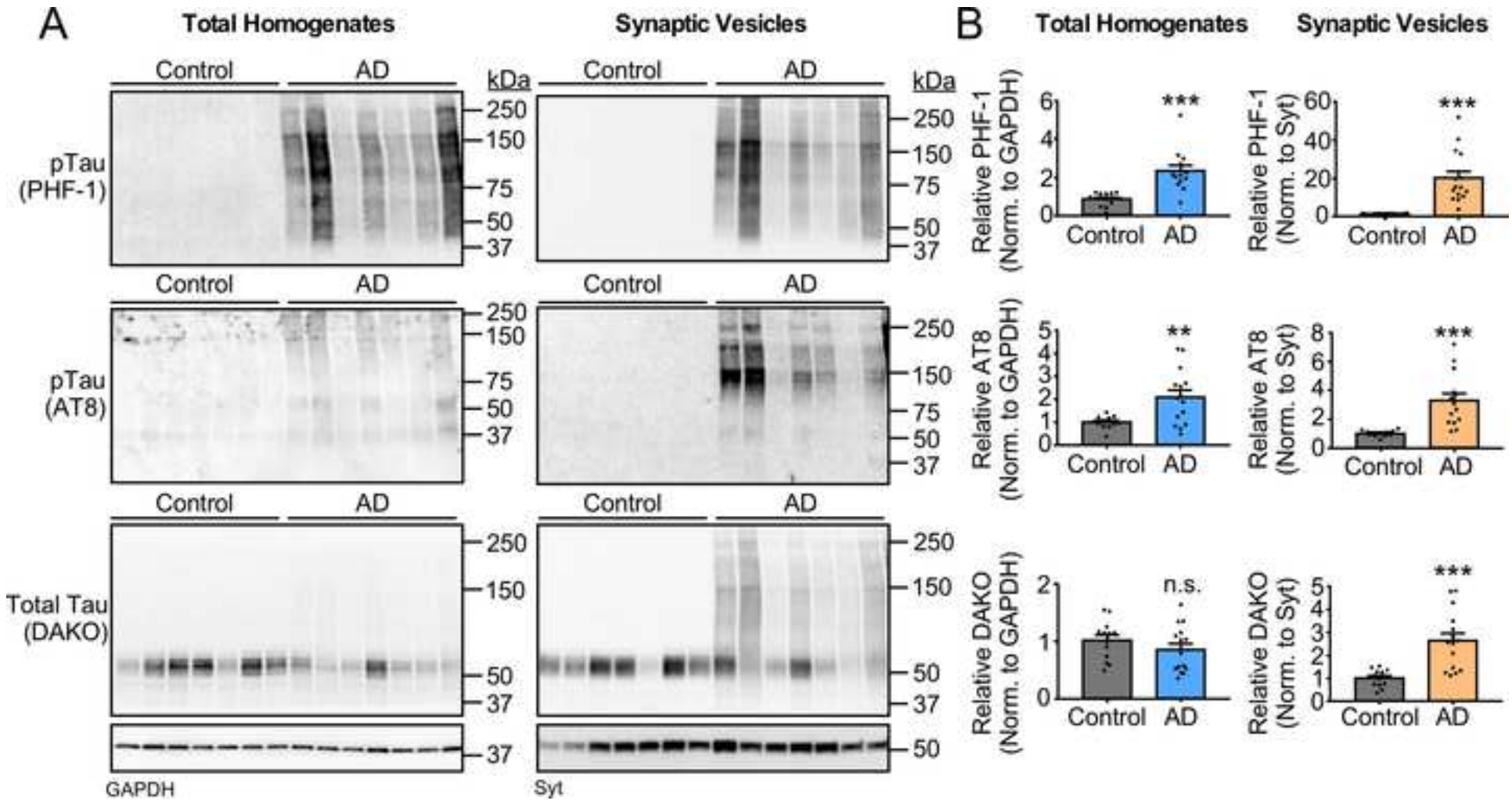

Figure 2

Click here to download Figure Fig 2.tif

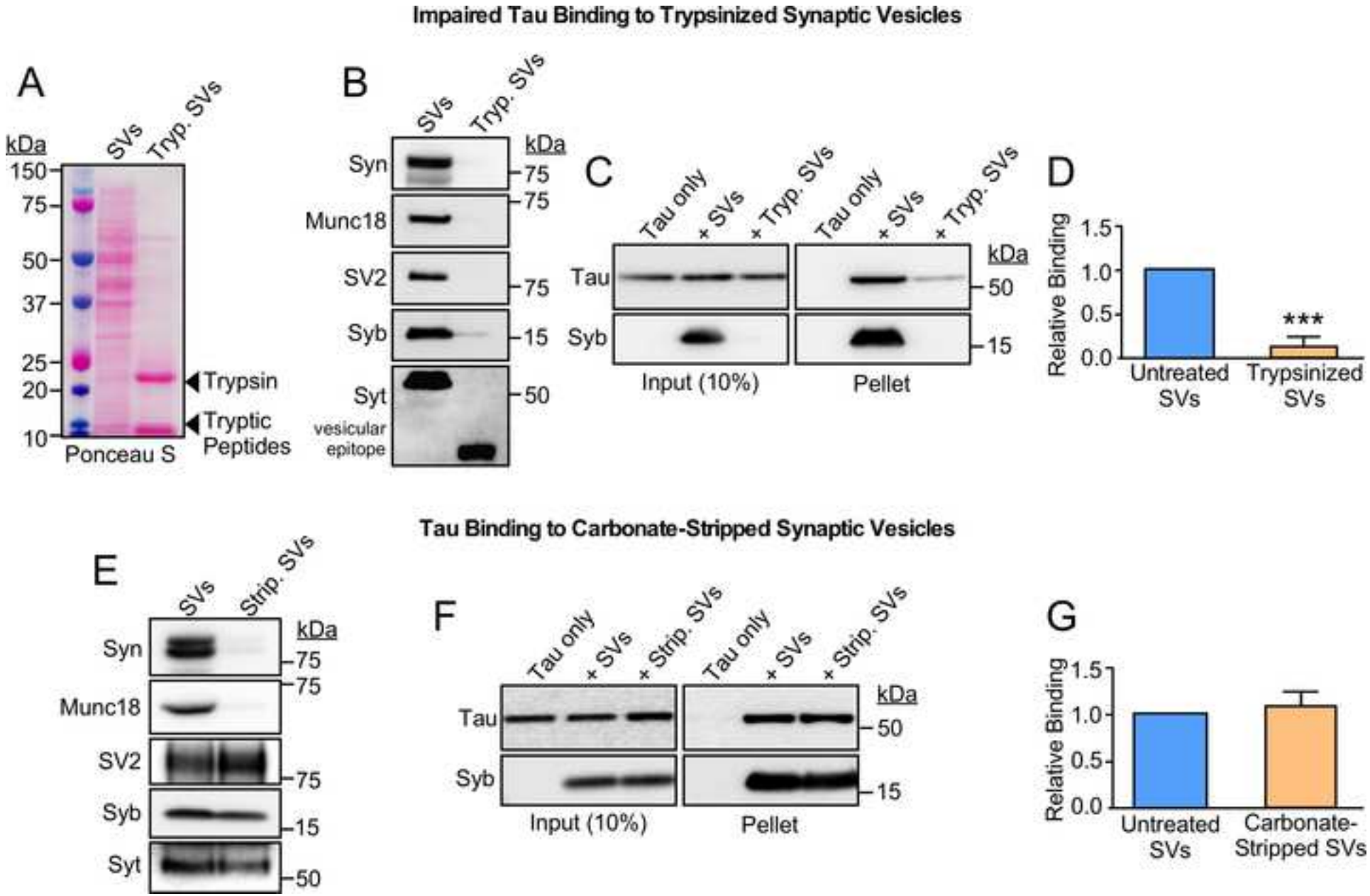

Figure 3

Identification of Synaptic Vesicle Interactor by Mass Spectrometry

A

Lyse isolated SVs in 2% Triton-X-100

↓

Incubate SV lysate with Tau^{FL}-His or $Tau^{\Delta N}$-His (IP: anti-His, 0.6% Triton-X-100)

↓

On-bead trypsin digestion

↓

Peptide analysis by LC-MS/MS

B

Protein	No. Peptides			*Drosophila* Homologue
	Neg.	Tau^{FL}	$Tau^{\Delta N}$	
Transmembrane SV Proteins				
Synaptogyrin-3	0	2	0	Syngr
Synaptotagmin-1	0	1	4	Syt
SV-Associated Proteins				
Synaptojanin-1	0	1	3	Synj
Rabphilin-3A	0	2	0	Rph
Dynamin-1	15	150	190	Shi
Dynamin-2	1	17	20	
Dynamin-3	0	33	37	
Septin-7	0	52	66	Pnut

Genetic Screen of Candidate Interactors *In Vivo* in *Drosophila*

C

Cross Tau^{P301L}-expressing flies to loss-of-function allele for candidate interactor

↓

Dissect larvae, fix and immunolabel Tau and SV marker (CSP)

↓

Confocal imaging of NMJs

↓

Unbiased quantification of colocalization coefficient between Tau and SVs

D

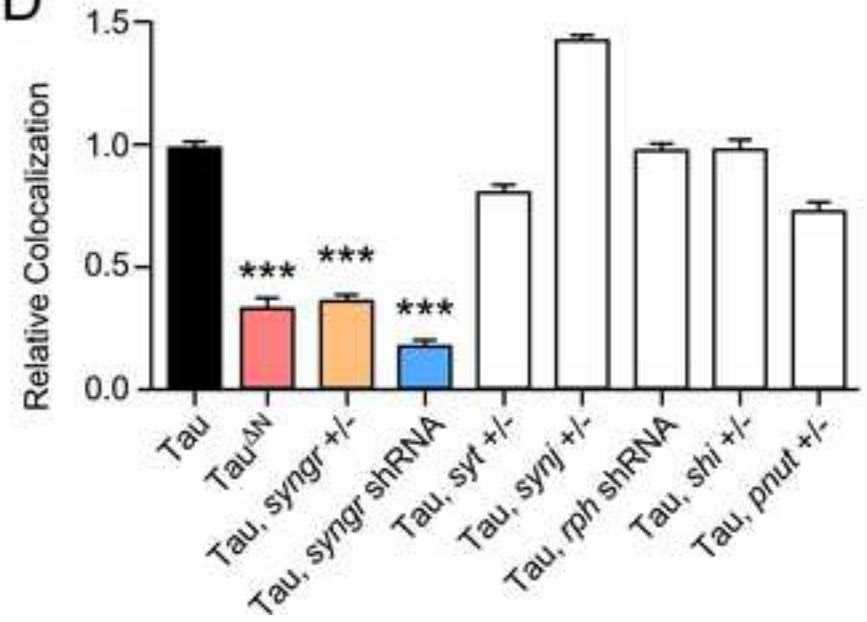

Figure 4

Click here to download Figure Fig 4.tif

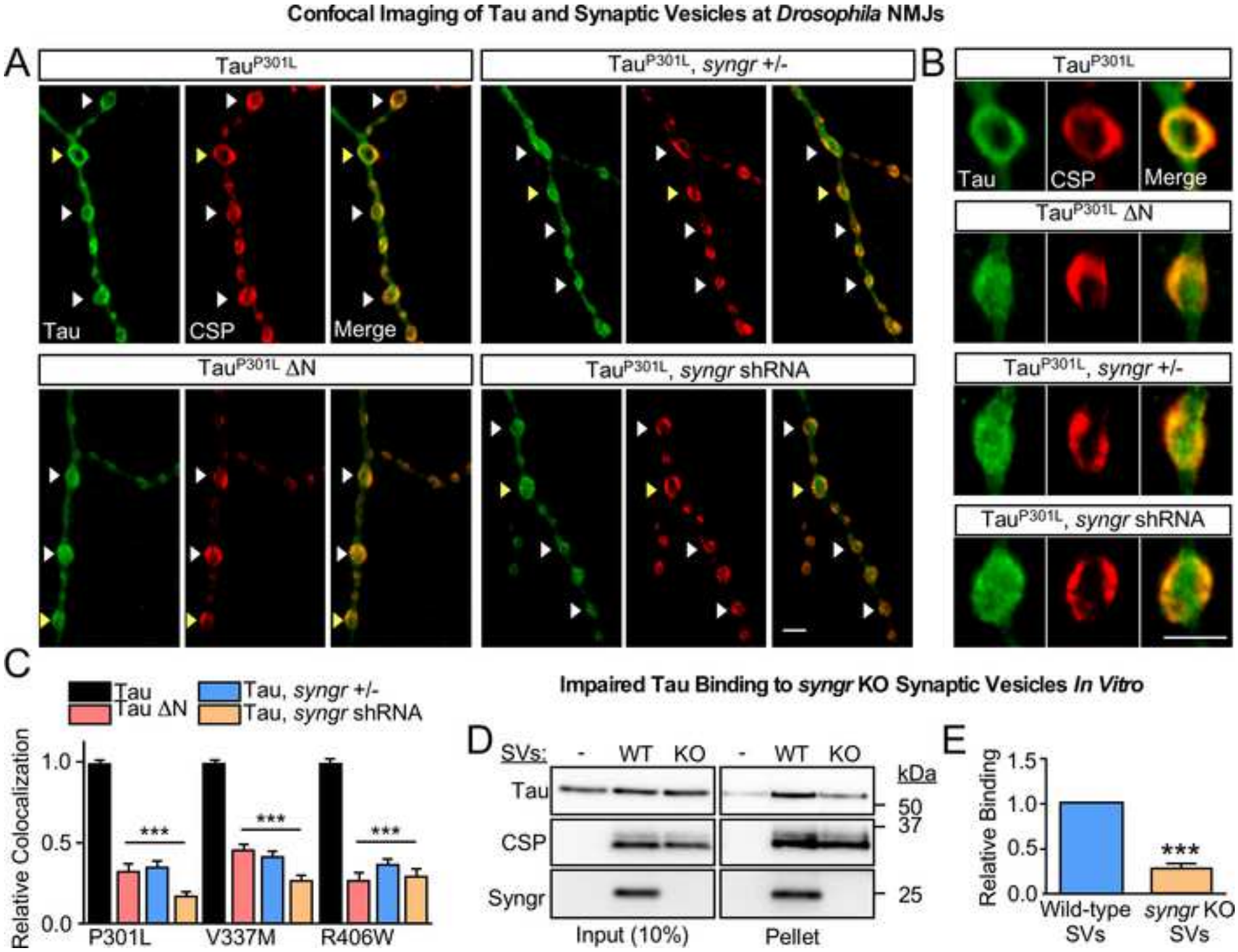

Figure 5

Click here to download Figure Fig 5.tif

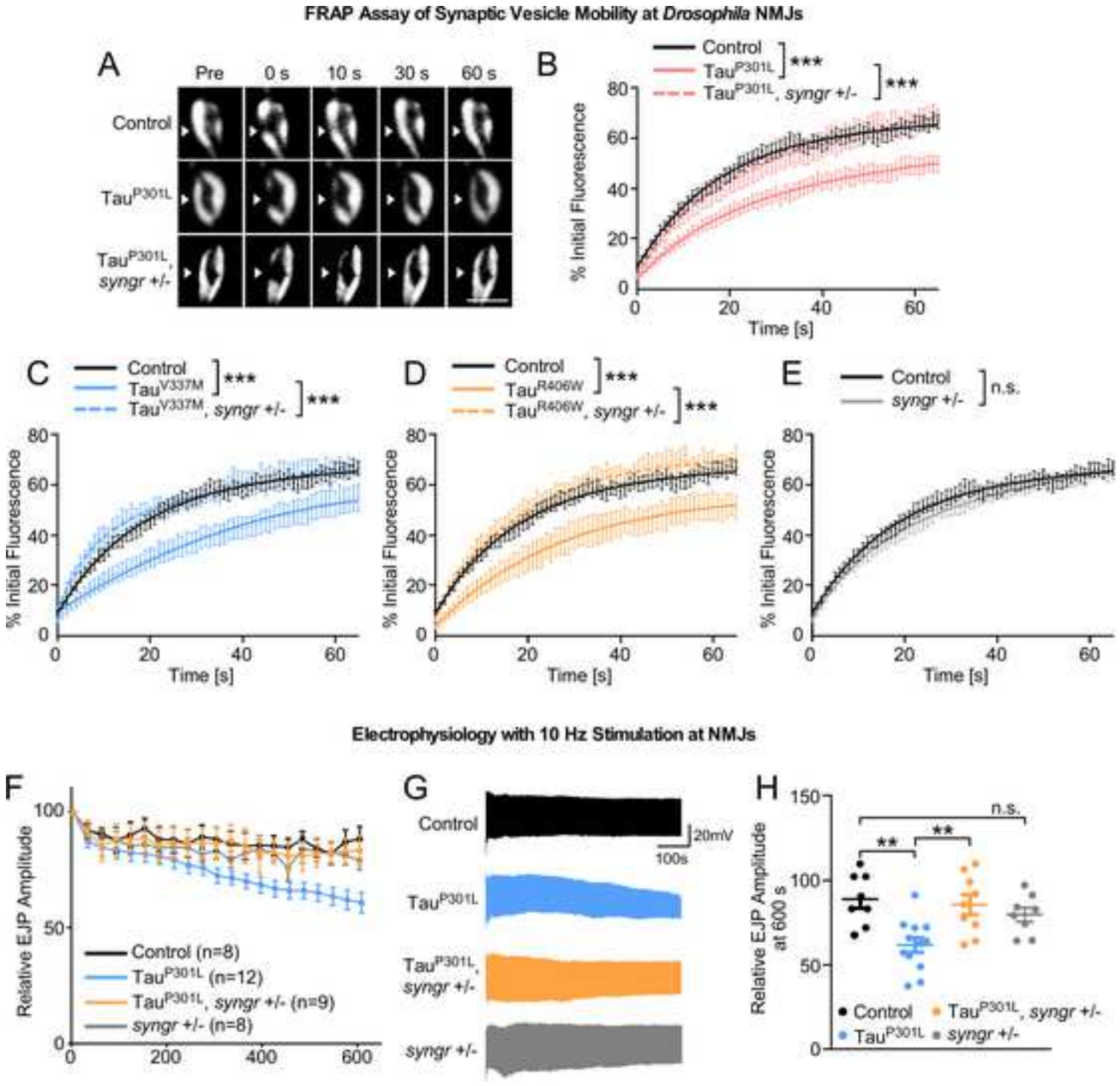

Figure 6

Click here to download Figure Fig 6.tif

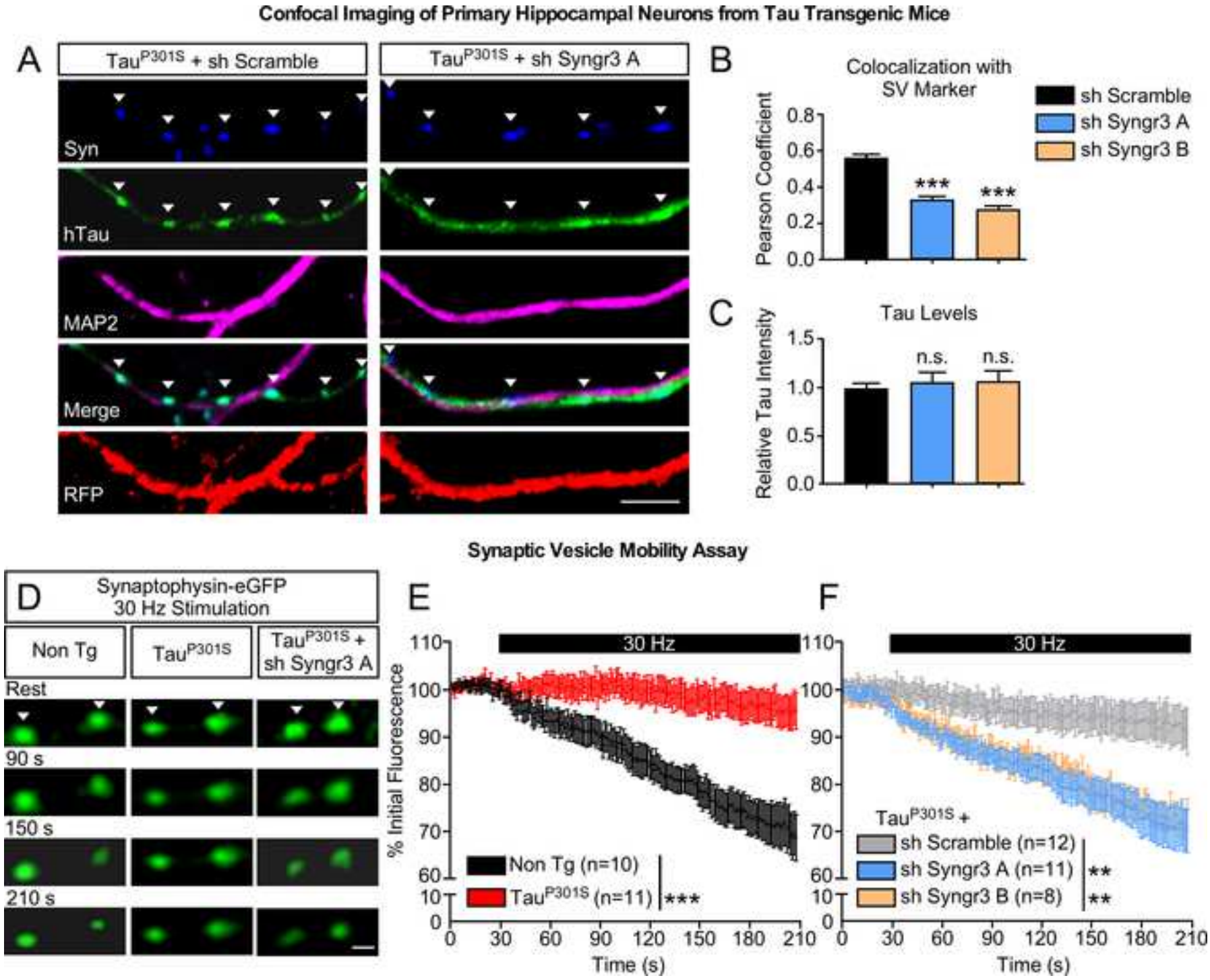

Figure 7

Click here to download Figure Fig 7.tif

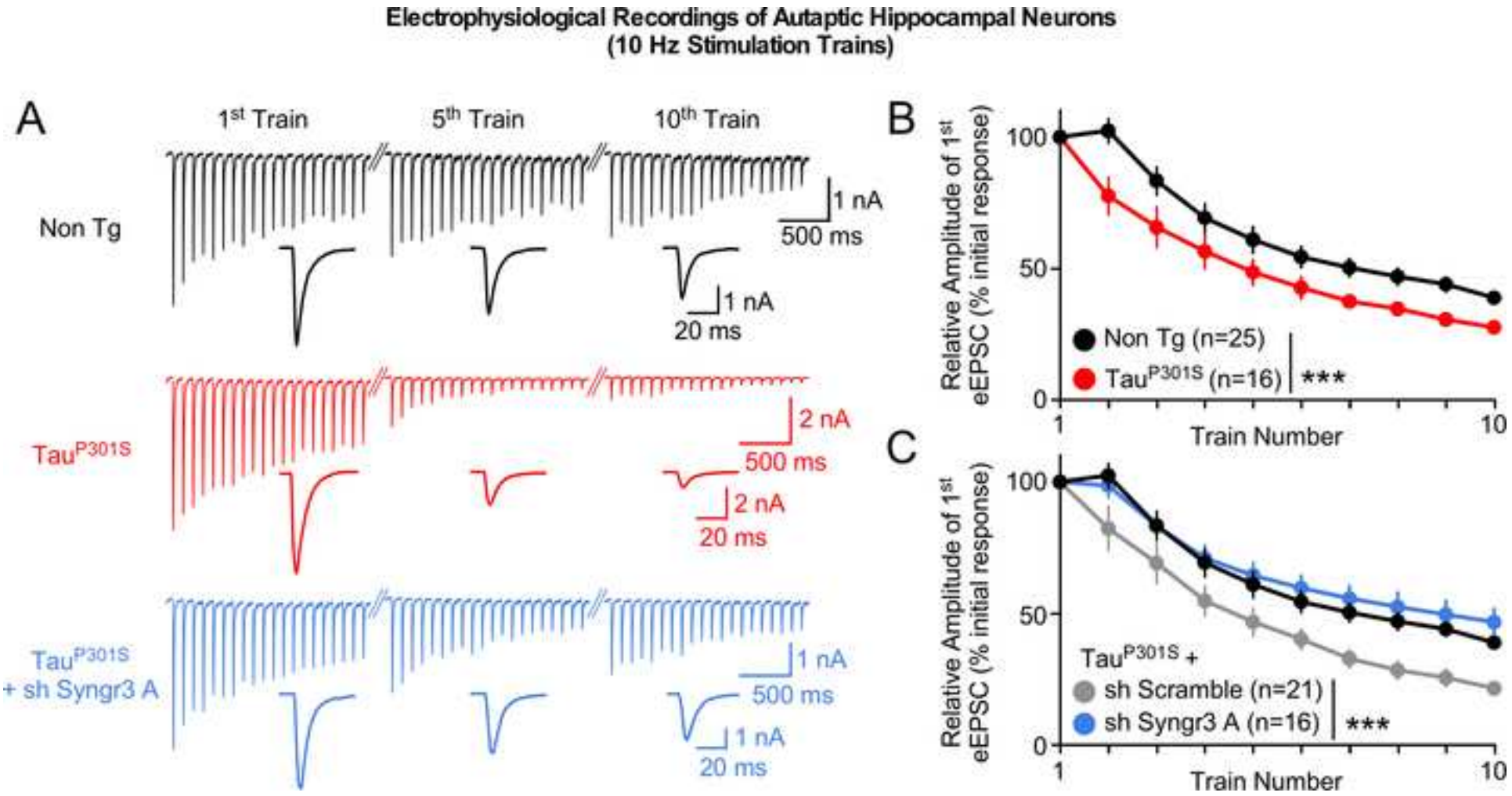

Figure S1

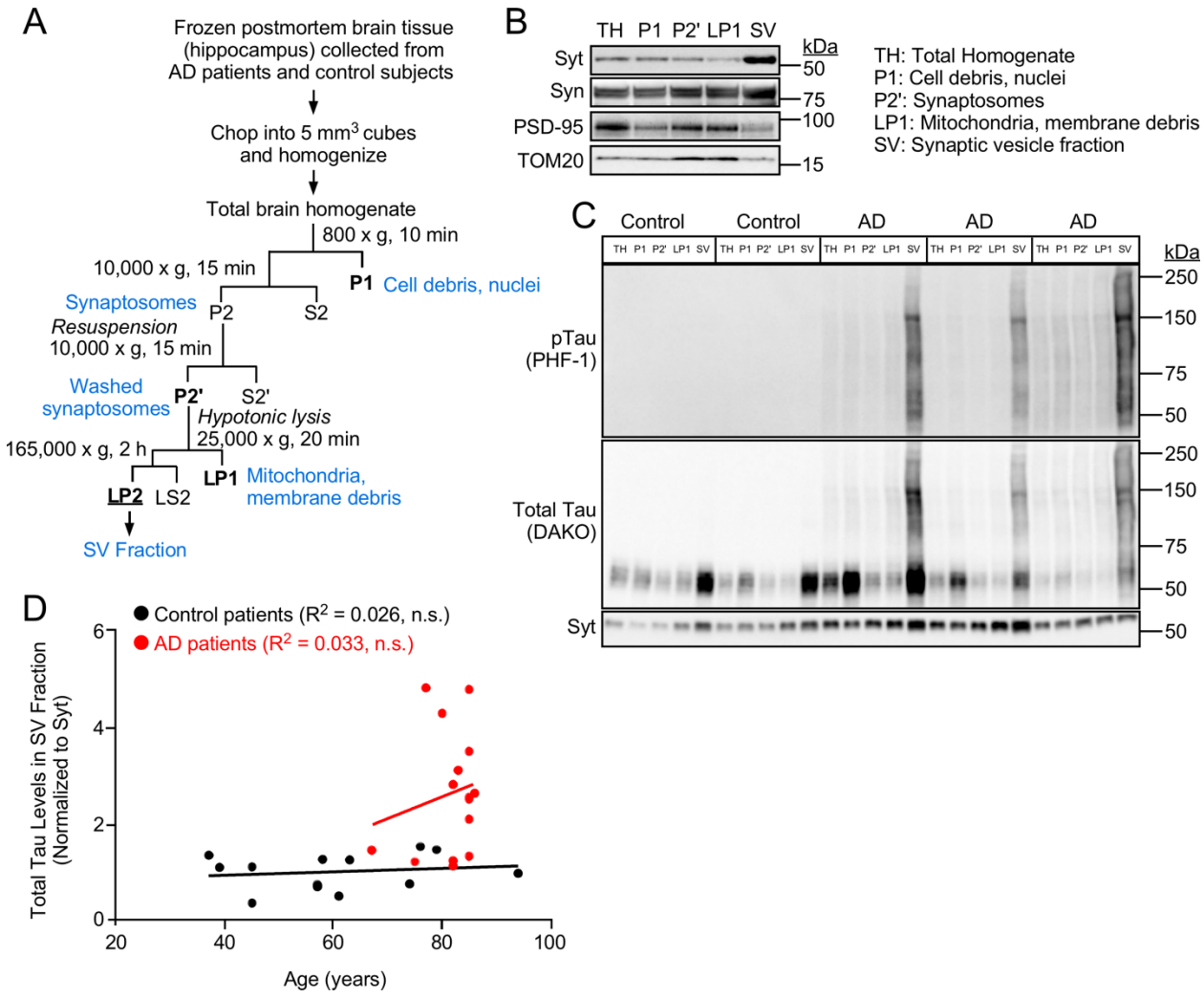

Figure S1. Related to Figure 1. (A) Schematic depicting isolation procedure of SVs from postmortem human brain tissue. (B) Representative immunoblots of fractions (20 µg protein of each fraction) collected during SV isolation from a non-demented control subject show enrichment of the SV markers Synaptotagmin-1 (Syt) and Synapsin-1 (Syn), and depletion of the post-synaptic marker PSD-95 and the mitochondrial marker TOM20. (C) Representative immunoblots detecting phospho-Tau (pTau) using PHF-1 antibody (phospho-Ser^{396}/Ser^{404} epitope) or total Tau (DAKO) antibody of representative subcellular fractions (20 µg protein of each fraction) collected during SV isolation from AD patient brains in comparison to control subject brains. Immunoblotting of Syt confirms enrichment of SVs in the SV fractions. (D) Plot of total Tau levels (DAKO antibody) on SVs in control and AD patients as a function of patient age. Correlation analysis was performed using a linear regression test in Prism software. n.s. – not significant.

Figure S2

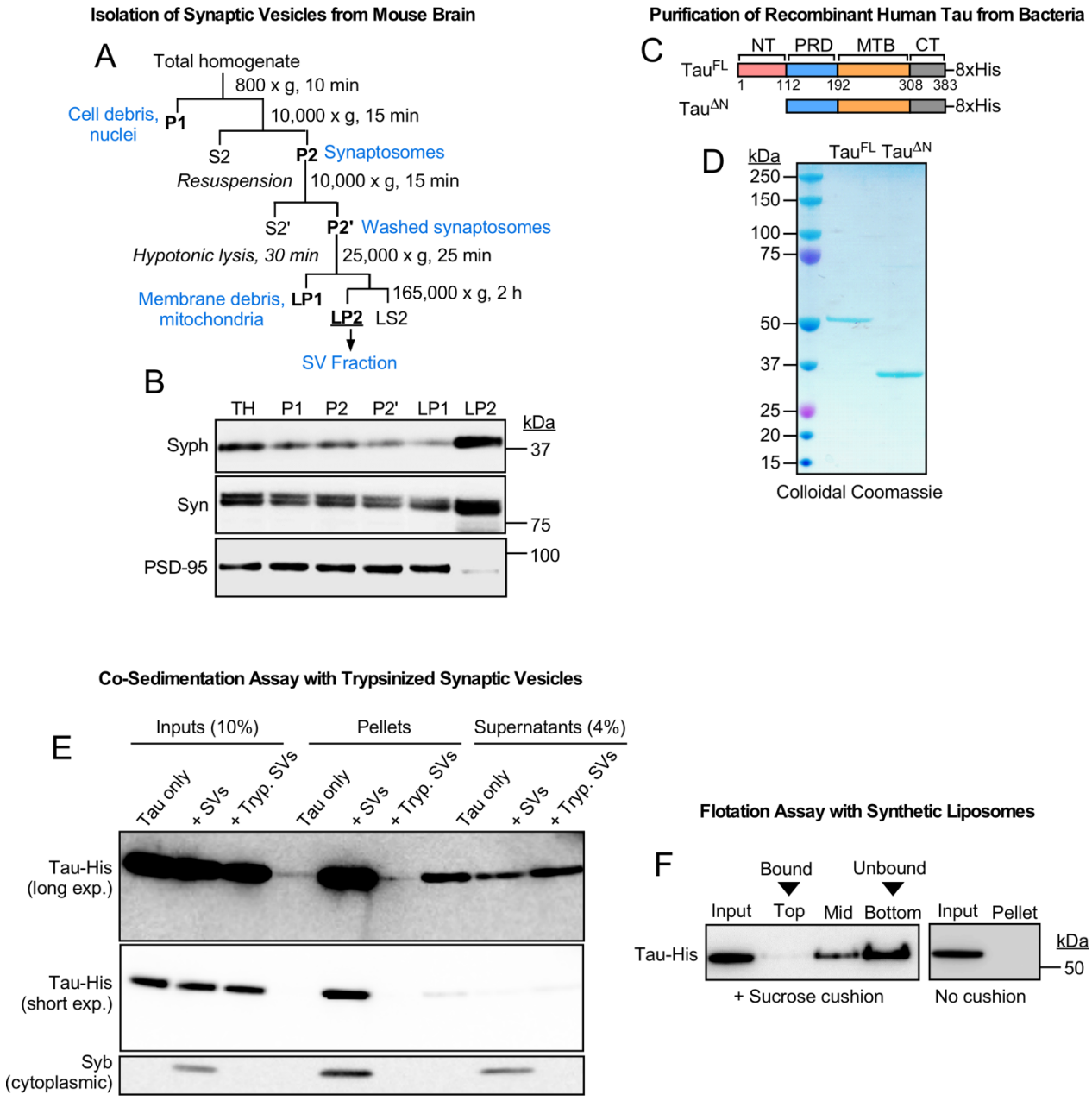
Isolation of Synaptic Vesicles from Mouse Brain
A
Total homogenate
800 x g, 10 min
Cell debris, nuclei
P1
10,000 x g, 15 min
S2
P2 Synaptosomes
Resuspension
10,000 x g, 15 min
S2'
P2' Washed synaptosomes
Hypotonic lysis, 30 min
25,000 x g, 25 min
Membrane debris, mitochondria
LP1
165,000 x g, 2 h
LP2
LS2
SV Fraction
B
TH P1 P2 P2' LP1 LP2
kDa
Syph
37
Syn
75
PSD-95
100
Purification of Recombinant Human Tau from Bacteria
C
NT PRD MTB CT
Tau^FL
8xHis
1 112 192 308 383
Tau^ΔN
8xHis
D
kDa
Tau^FL Tau^ΔN
250
150
100
75
50
37
25
20
15
Colloidal Coomassie
Co-Sedimentation Assay with Trypsinized Synaptic Vesicles
E
Inputs (10%)
Pellets
Supernatants (4%)
Tau only
+ SVs
+ Tryp. SVs
Tau-His (long exp.)
Tau-His (short exp.)
Syb (cytoplasmic)
Flotation Assay with Synthetic Liposomes
F
Bound
Unbound
Input Top Mid Bottom Input Pellet
kDa
Tau-His
50
+ Sucrose cushion
No cushion

Figure S2. Related to Figure 2. (A-B) Isolation of synaptic vesicles from mouse brain. (A) Schematic depicting isolation procedure of SVs from mouse brain. (B) Immunoblotting of fractions collected during SV isolation (20 µg protein of each fraction) shows the SV fraction (LP2) is enriched for the SV markers Synaptophysin-1 (Syph) and Synapsin-1 (Syn) and depleted of the postsynaptic marker PSD-95. **(C-D) Purification of recombinant human Tau.** (C) Schematic depicting 8xHis-tagged full-length (FL, aa 1-383) and N-terminally truncated (ΔN, aa 113-383) Tau proteins (0N4R isoform). (D) Colloidal Coomassie staining (1 µg protein) of recombinant Tau^{FL}-8xHis or $Tau^{\Delta N}$-8xHis purified from bacterial cultures. **(E) Immunoblots of supernatant fractions from SV co-sedimentation assay.** Note that Tau persists in the supernatant of the trypsinized SV binding reaction., confirming that there is no residual trypsin activity degrading recombinant Tau (anti-His antibody) in the Tau + trypsinized SVs binding reaction. **(F) Co-flotation assay of recombinant Tau and liposomes.** Tau and liposomes were incubated together, then covered by a sucrose cushion and centrifuged. Due to their density, liposomes rise to the top fraction of the sucrose cushion after centrifugation. Left panel: Representative immunoblot showing that recombinant Tau (anti-His antibody) does not rise to the top fraction together with liposomes in a co-flotation assay, indicating a lack of binding. Each fraction was loaded in equal volumes. Right panel: The retention of Tau in the bottom fraction is not due to the pelleting of Tau (e.g. due to aggregation), as Tau alone does not pellet in the absence of a sucrose cushion. Inputs are 10%.

Figure S3

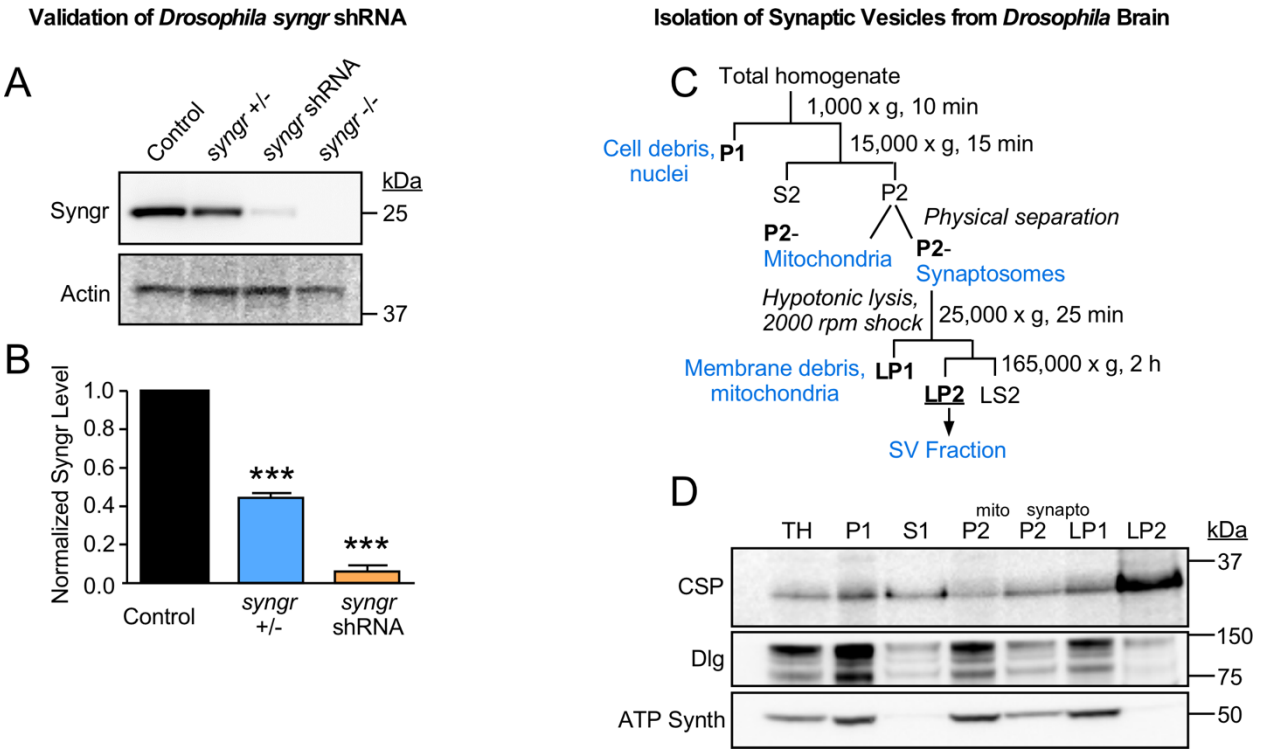

Figure S3. Related to Figure 4. (A-B) Knockdown efficiency of *Drosophila syngr* shRNA. (A) Representative immunoblot of Syngr levels in protein lysates from adult fly brain, as quantified in (B). Protein levels were normalized to Actin loading control. Wild-type w1118 flies were used as controls. *Syngr*$^{+/-}$ and *syngr*$^{-/-}$ serve as controls for antibody specificity. The UAS-*syngr* shRNA is expressed using the pan-neuronal nSyb-Gal4 driver. Graph depicts mean ± SD (n = 3 experiments, one-way ANOVA, *** $p < 0.001$). **(C-D) Isolation of synaptic vesicles from adult *Drosophila* brain.** (C) Schematic depicting isolation procedure of SVs from adult *Drosophila* brain. (D) Representative immunoblots of fractions collected during SV isolation (20 µg protein of each fraction) show that the SV fraction is enriched for the SV marker Cysteine String Protein (CSP), and depleted of the postsynaptic marker Discs-large (Dlg) and the mitochondrial marker ATP synthase.

Figure S4

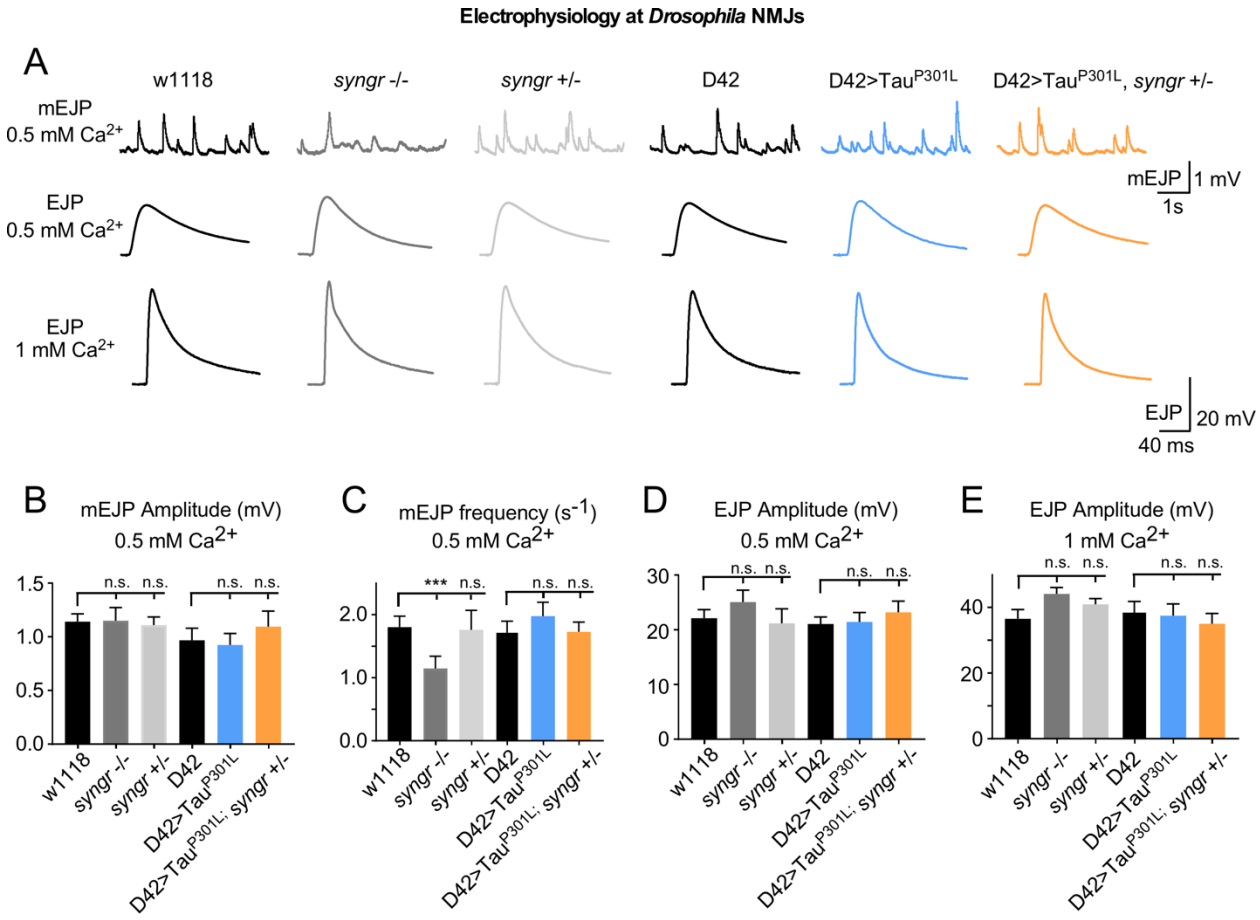

Figure S4. Analysis of basal neurotransmitter release at *Drosophila* NMJs. Related to Figure 5. (A) Representative traces of spontaneous miniature excitatory junction potentials (mEJP) or evoked excitatory junction potentials (EJP) at 0.5 mM or 1 mM Ca^{2+}, as indicated. w1118 is control for *syngr* mutant background; D42-Gal4 driver only is control for D42 > Tau^{P301L} and D42 > Tau^{P301L}, $syngr^{+/-}$ genotypes. (B-C) Quantifications of mEJP amplitude (B) and frequency (C). (D-E) Quantification of EJP amplitudes averaged from 1 min stimulation at 0.2 Hz in buffer containing 0.5 mM Ca^{2+} (D) or 1 mM Ca^{2+} (E). In (B-E) graphs depict mean ± SEM (n $\geq$ 7 NMJs from $\geq$ 5 animals per genotype, one-way ANOVA, *** $p < 0.001$, n.s. – not significant).

Figure S5

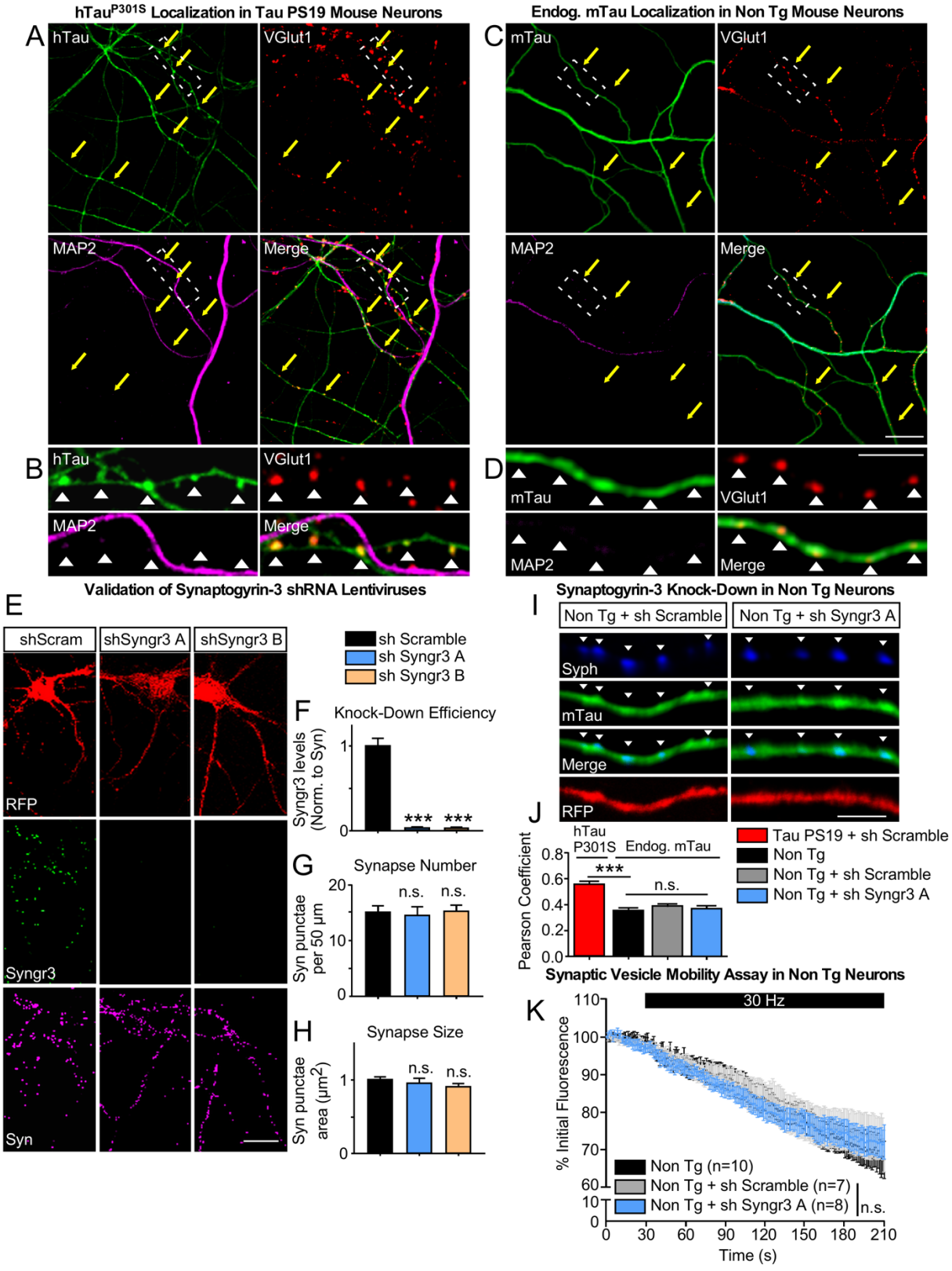
hTauP301S Localization in Tau PS19 Mouse Neurons
Endog. mTau Localization in Non Tg Mouse Neurons
A
hTau
VGlut1
MAP2
Merge
C
mTau
VGlut1
MAP2
Merge
B
hTau
VGlut1
MAP2
Merge
D
mTau
VGlut1
MAP2
Merge
Validation of Synaptogyrin-3 shRNA Lentiviruses
E
shScram
shSyngr3 A
shSyngr3 B
RFP
Syngr3
Syn
sh Scramble
sh Syngr3 A
sh Syngr3 B
F
Knock-Down Efficiency
Syngr3 levels (Norm. to Syn)
***
***
G
Synapse Number
Syn punctae per 50 µm
n.s.
n.s.
H
Synapse Size
Syn punctae area (µm2)
n.s.
n.s.
Synaptogyrin-3 Knock-Down in Non Tg Neurons
I
Non Tg + sh Scramble
Non Tg + sh Syngr3 A
Syph
mTau
Merge
RFP
J
hTau P301S
Endog. mTau
***
n.s.
Pearson Coefficient
Tau PS19 + sh Scramble
Non Tg
Non Tg + sh Scramble
Non Tg + sh Syngr3 A
Synaptic Vesicle Mobility Assay in Non Tg Neurons
K
30 Hz
% Initial Fluorescence
Non Tg (n=10)
Non Tg + sh Scramble (n=7)
Non Tg + sh Syngr3 A (n=8)
n.s.
Time (s)

Figure S5. Related to Figure 6. (A-D) Tau localization in primary hippocampal neurons from Tau PS19 (Tau^{P301S}) transgenic mice and Non Tg mice. Representative immunolabeling of human Tau^{P301S} (hTau, HT7 antibody) or endogenous mouse Tau (mTau, DAKO antibody) in DIV17 primary neurons from Tau PS19 mice (A-B) or Non Tg mice (C-D). VGlut1 and MAP2 labeling serve as presynaptic and dendritic markers, respectively. Note that hTau^{P301S} displays a punctate colocalization with the presynaptic marker VGlut1 along distal axons of Tau PS19 neurons (A-B), while endogenous mTau displays a diffuse staining pattern along the axon (C-D). Yellow arrows indicate regions of presynaptic VGlut1 puncta along axons. Scale bar is 15 μm. (B, D) Higher magnifications of axonal segments depicted in boxes in (A, C). White arrowheads indicate presynaptic VGlut1 puncta. Scale bar is 5 μm. **(E-H) Validation of Synaptogyrin-3 knockdown using lentiviruses encoding Synaptogyrin-3 shRNAs.** Primary neurons were transduced on DIV5 with lentivirus encoding RFP and scrambled or Syngr3 shRNAs, then fixed on DIV11 and immunolabeled for Synaptogyrin-3 (Syngr3) and Synapsin-1 (Syn). (E) Representative images of primary neurons transduced with lentivirus expressing RFP and encoding either scramble or Syngr3 shRNAs. Scale bar is 25 μm. (F) Quantification of Syngr3 levels. Synapses were identified by Syn labeling, and each synapse was measured for Syngr3 and Syn intensity. Syngr3 intensity at each puncta was normalized to Syn intensity, and all synaptic puncta were averaged to give the mean Syngr3 intensity value per axon/cell. Graph depicts mean ± SEM (n = 50 axons from $\geq$ 12 coverslips from 3 independent cultures, one-way ANOVA, *** $p < 0.001$). (G) The number of synapses along axons of transduced neurons was measured as the number of Syn puncta per 50 μm of axon length. (H) Synapse size was measured by averaging the area of each Syn puncta along an axon to give the mean synapse size for each axon/cell. In (G-H) graphs depict mean ± SEM (n = 20 axons/cells, one-way ANOVA, n.s. – not significant). **(I-J) The staining pattern of endogenous mTau is not affected upon Synaptogyrin-3 knockdown in Non Tg neurons.** (I) Representative confocal images of Non Tg neurons transduced with scrambled or Syngr3 knockdown lentivirus and immunolabeled for endogenous mouse Tau (mTau, DAKO antibody) and the SV marker Synaptophysin-1 (Syph). White arrowheads indicate presynaptic Syph puncta along axons. Scale bar is 5 μm. (J) Quantification of Tau colocalization with the presynaptic SV marker Syph was calculated as the Pearson Coefficient of either hTau^{P301S} in Tau PS19 neurons or WT mTau in Non Tg neurons in various conditions, as indicated. Graph depicts mean ± SEM (n = 80 axons/cells, one-way ANOVA, *** $p < 0.001$, n.s. – not significant). **(K) Synaptic vesicle mobility in Non Tg neurons is not affected by Synaptogyrin-3 knockdown.** Plot depicting change in Syph-eGFP fluorescence intensity in response to 30 Hz stimulation in Non Tg neurons co-transduced with Syph-eGFP lentivirus and scrambled or Syngr3 knockdown lentivirus. Plot depicts mean ± SEM (n recordings indicated, two-way ANOVA, n.s. – not significant).

Figure S6

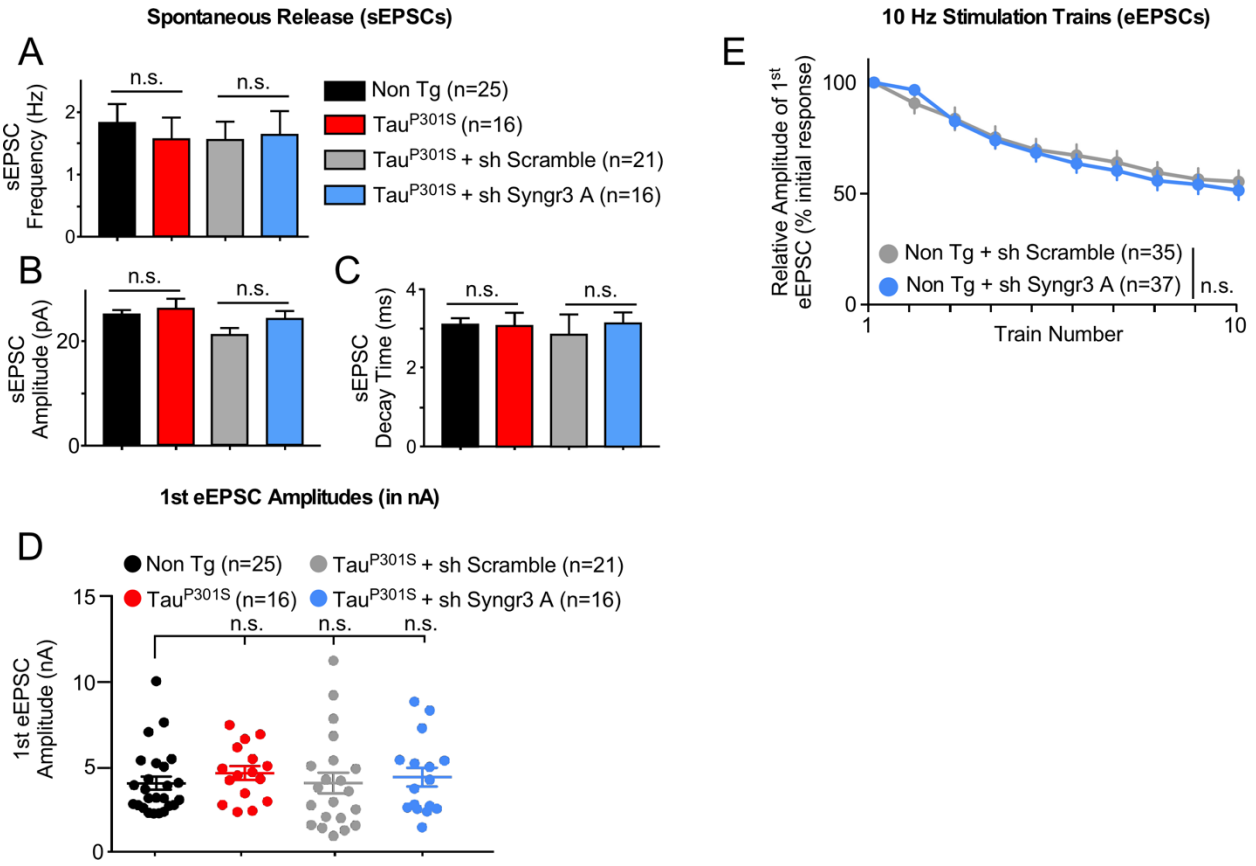

Figure S6. Related to Figure 7. (A-C) Analysis of spontaneous neurotransmitter release in Non Tg and Tau PS19 neurons. Autaptic neuronal cultures were established from Non Tg or Tau PS19 littermate mice and transduced with lentivirus as indicated. Spontaneous excitatory post-synaptic currents (sEPSCs) were recorded on DIV17-20 in 4 mM Ca^{2+}. Plots depict mean ± SEM of sEPSC frequency (A), amplitude (B), and decay time (C) (n recordings indicated, Student's t-test, n.s. – not significant). **(D) Baseline evoked release is not affected among Non Tg, Tau^{P301S} and Tau^{P301S} + Syngr3 knockdown neuron genotypes.** Plot of raw 1st evoked eEPSC amplitudes from Figure 7 plotted as nA. Data points represent individual recordings from n neurons, indicated. One-way ANOVA; n.s – not significant. **(E) Evoked neurotransmitter release in Non Tg neurons is not affected upon Synaptogyrin-3 knockdown.** Recordings of autaptic hippocampal neurons in response to 10 consecutive high frequency stimulation trains (10 Hz for 10 s with 30 s intervals, 4 mM Ca^{2+}). Plot depicts mean ± SEM of %1st evoked response (n recordings indicated from ≥ 3 independent cultures, some error bars too small to be seen, two-way ANOVA, n.s. – not significant).

Table S1. Patient data for human brain samples related to Figure 1.

Internal Reference	Age	Gender	Diagnosis	Braak Stage	MRC Database No. (BBN)
Control Group					
BD 2010-062	94	Female	ND	-	N/A
BD 2010-038	79	Female	ND	-	N/A
Ed2 SD055/12	76	Male	ND	-	9508
Ed2 SD014/13	74	Female	ND	-	14395
Ed2 SD048/12	63	Male	ND	-	7626
Ed2 SD032/13	61	Male	ND	-	16425
Ed1 SD029/13	58	Male	ND	-	15809
Ed1 SD011/15	57	Male	ND	-	24781
Ed1 SD010/15	57	Female	ND	-	24780
Ed1 SD017/13	45	Female	ND	-	14397
Ed1 SD022/13	45	Male	ND	-	15222
Ed1 SD022/16	39	Male	ND	-	28959
Ed1 SD026/16	37	Female	ND	-	28960
AD Group					
Ed1 SD013/13	86	Male	AD	4	15812
Ed2 SD033/14	85	Female	AD	3	22627
Ed2 SD045/13	85	Female	AD	3	19600
Ed2 SD035/13	85	Female	AD	4	18798
Ed1 SD033/14	85	Female	AD	3	22627
Ed1 SD045/13	85	Female	AD	3	19600
Ed1 SD035/13	85	Female	AD	4	18798
Ed1 SD046/14	83	Female	AD	3	24306
BD 2007-009	82	Female	AD	4	N/A
Ed2 SD019/13	82	Female	AD	4	15814
Ed1 SD019/13	82	Female	AD	4	15814
BD 2010-011	80	Male	AD	4	N/A
Ed2 SD023/15	77	Male	AD	3	26491
Ed1 SD017/14	75	Male	AD	3	20994
Ed2 SD050/14	67	Male	AD	4	24323

Table S2. Complete mass spectrometry dataset from co-IP of Tau^{FL}-His and Tau$^{\Delta N}$-His with synaptic vesicle lysate. Related to Figure 3. Proteins identified were cross-referenced against previous data sets defining the synaptic vesicle proteome, and proteins were classified as transmembrane SV proteins, SV-associated proteins, or others (contaminates). Spectral counts are given from three technical replicates.

Accession	Description	Gene Name	Spectral Counts IgG only			Spectral Counts Tau^{FL}-His			Spectral Counts Tau$^{\Delta N}$-His		
	Transmembrane synaptic vesicle proteins										
Q8R191	Synaptogyrin-3	Syngr3	0	0	0	0	1	1	0	0	0
P46096	Synaptotagmin-1	Syt1	0	0	0	1	0	0	0	1	3
	Peripheral synaptic vesicle-associated proteins										
Q8CHC4	Synaptojanin-1	Synj1	0	0	0	0	1	0	0	2	1
P47708	Rabphilin-3A	Rph3a	0	0	0	2	0	0	0	0	0
P39053	Dynamin-1	Dnm1	5	5	5	50	46	54	67	65	58
P39054	Dynamin-2	Dnm2	0	0	1	5	5	7	5	5	0
Q8BZ98	Dynamin-3	Dnm3	0	0	0	10	14	9	13	9	15
O55131	Septin-7	Sept7	0	0	0	19	15	18	22	23	21
O88935	Synapsin-1	Syn1	47	51	50	26	20	22	12	15	12
Q64332	Synapsin-2	Syn2	1	1	0	1	0	2	0	1	2
Q9QYX7	Protein piccolo	Pclo	1	0	0	0	0	0	0	0	0
	Other non-synaptic vesicle proteins (absent in negative control)										
Q9Z2Q6	Septin-5	Sept5	0	0	0	8	9	10	6	9	7
Q8QZT1	Acetyl-CoA acetyltransferase, mitochondrial	Acat1	0	0	0	8	9	7	9	10	10
Q8BYI9	Tenascin-R	Tnr	0	0	0	7	9	4	1	0	1
Q8C1B7	Septin-11	Sept11	0	0	0	7	8	4	7	8	8
Q9R1T4	Septin-6	Sept6	0	0	0	7	5	6	7	7	6
Q9Z1S5	Neuronal-specific septin-3	Sept3	0	0	0	6	7	5	7	6	4
Q5SQX6	Cytoplasmic FMR1-interacting protein 2	Cyfip2	0	0	0	3	1	2	2	1	2
Q80UG5	Septin-9	Sept9	0	0	0	2	3	4	4	5	4
Q8CBW3	Abl interactor 1	Abi1	0	0	0	2	3	2	7	4	5
Q8R5H6	Wiskott-Aldrich syndrome protein family member 1	Wasf1	0	0	0	2	1	3	4	1	1
Q8CHH9	Septin-8	Sept8	0	0	0	2	1	2	2	1	1
P62281	40S ribosomal protein S11	Rps11	0	0	0	1	2	1	0	0	0
P62484	Abl interactor 2	Abi2	0	0	0	1	2	0	2	0	3
P47754	F-actin-capping protein subunit alpha-2	Capza2	0	0	0	1	1	1	3	1	2
P28660	Nck-associated protein 1	Nckap1	0	0	0	1	1	1	2	2	2
Q8R550	SH3 domain-containing kinase-binding protein 1	Sh3kbp1	0	0	0	1	1	1	1	1	1

P62631	Elongation factor 1-alpha 2	Eef1a2	0	0	0	1	1	1	0	1	1
P42208	Septin-2	Sept2	0	0	0	1	1	0	1	1	1
P99024	Tubulin beta-5 chain	Tubb5	0	0	0	1	1	0	1	1	0
Q60737	Casein kinase II subunit alpha	Csnk2a1	0	0	0	1	1	0	0	1	1
P68372	Tubulin beta-4B chain	Tubb4b	0	0	0	1	0	0	1	0	0
P42669	Transcriptional activator protein Pur-alpha	Pura	0	0	0	1	0	0	0	0	0
P80314	T-complex protein 1 subunit beta	Cct2	0	0	0	0	2	0	0	0	0
P59644	Phosphatidylinositol 4,5-bisphosphate 5-phosphatase A	Inpp5j	0	0	0	0	1	1	0	0	0
P14873	Microtubule-associated protein 1B	Map1b	0	0	0	0	1	0	0	0	0
P62267	40S ribosomal protein S23	Rps23	0	0	0	0	1	0	0	0	0
P62301	40S ribosomal protein S13	Rps13	0	0	0	0	1	0	0	0	0
Q6H1V1	Bestrophin-3	Best3	0	0	0	0	1	0	0	0	0
P28661	Septin-4	Sept4	0	0	0	0	0	1	1	0	1
P59999	Actin-related protein 2/3 complex subunit 4	Arpc4	0	0	0	0	0	1	0	0	0
Q3UJD6	Ubiquitin carboxyl-terminal hydrolase 19	Usp19	0	0	0	0	0	1	0	0	0
Q62086	Serum paraoxonase/arylesterase 2	Pon2	0	0	0	0	0	1	0	0	0
Q812A2	SLIT-ROBO Rho GTPase-activating protein 3	Srgap3	0	0	0	0	0	0	1	0	0
P62082	40S ribosomal protein S7	Rps7	0	0	0	0	0	0	0	1	0
P63085	Mitogen-activated protein kinase 1	Mapk1	0	0	0	0	0	0	0	0	1
Q91VR8	Protein BRICK1	Brk1	0	0	0	0	0	0	0	0	1
	Other non-synaptic vesicle proteins (present in negative control)										
P20357	Microtubule-associated protein 2	Map2	23	15	21	19	16	12	11	9	6
P04370	Myelin basic protein	Mbp	14	13	13	13	13	11	10	12	10
P27546	Microtubule-associated protein 4	Map4	11	12	10	5	4	6	4	2	2
P16858	Glyceraldehyde-3-phosphate dehydrogenase	Gapdh	9	9	5	13	8	10	9	8	11
Q6PEV3	WAS/WASL-interacting protein family member 2	Wipf2	8	9	7	1	1	0	0	0	0
E9Q6B2	Coiled-coil domain-containing protein 85C	Ccdc85c	6	4	5	0	0	0	0	0	0
Q61191	Host cell factor 1	Hcfc1	6	3	5	0	0	0	0	0	0
P02535	Keratin, type I cytoskeletal 10	Krt10	5	4	5	1	1	2	2	3	2
Q7TQD2	Tubulin polymerization-promoting protein	Tppp	4	4	5	3	4	3	2	1	4
P14131	40S ribosomal protein S16	Rps16	4	3	3	2	1	1	1	1	1
P62862	40S ribosomal protein S30	Fau	3	2	3	1	1	2	1	3	2
P10126	Elongation factor 1-alpha 1	Eef1a1	2	3	3	3	3	2	3	2	2
Q7TSJ2	Microtubule-associated protein 6	Map6	2	3	3	1	0	0	1	0	1
Q3TTY5	Keratin, type II cytoskeletal 2 epidermal	Krt2	2	2	2	0	0	1	0	0	0
Q8CC35	Synaptopodin	Synpo	2	2	1	0	0	0	0	0	0

P04104	Keratin, type II cytoskeletal 1	Krt1	2	1	2	0	0	0	1	1	1
P62274	40S ribosomal protein S29	Rps29	2	1	1	1	1	1	0	1	1
P62259	14-3-3 protein epsilon	Ywhae	2	0	1	0	0	1	0	0	0
P08730	Keratin, type I cytoskeletal 13	Krt13	1	2	2	0	0	0	0	0	0
P07724	Serum albumin	Alb	1	2	1	1	1	0	1	1	1
P62270	40S ribosomal protein S18	Rps18	1	1	3	4	7	4	1	3	2
P15105	Glutamine synthetase	Glul	1	1	1	2	2	1	1	1	1
P50446	Keratin, type II cytoskeletal 6A	Krt6a	1	1	1	1	1	1	1	1	1
P02088	Hemoglobin subunit beta-1	Hbb-b1	1	1	1	1	0	1	1	1	1
P28665	Murinoglobulin-1	Mug1	1	1	1	0	0	0	1	1	0
Q3UV17	Keratin, type II cytoskeletal 2 oral	Krt76	1	1	1	0	0	0	1	1	0
P01868	Ig gamma-1 chain C region secreted form	Ighg1	1	1	1	0	0	0	0	0	0
P97315	Cysteine and glycine-rich protein 1	Csrp1	1	1	0	1	1	1	1	0	0
Q8VED5	Keratin, type II cytoskeletal 79	Krt79	1	1	0	1	0	0	1	0	1
D3YZU1	SH3 and multiple ankyrin repeat domains protein 1	Shank1	1	1	0	0	0	0	0	0	0
P0CG14	Chromosome transmission fidelity protein 8 homolog isoform 2	Chtf8	1	0	1	0	0	0	0	0	0
Q91YD9	Neural Wiskott-Aldrich syndrome protein	Wasl	1	0	1	0	0	0	0	0	0
P05213	Tubulin alpha-1B chain	Tuba1b	1	0	0	1	1	1	1	1	1
Q3U3V8	X-ray radiation resistance-associated protein 1	Xrra1	1	0	0	1	1	1	1	1	1
A2AQ07	Tubulin beta-1 chain	Tubb1	1	0	0	1	1	1	0	1	0
P62702	40S ribosomal protein S4, X isoform	Rps4x	1	0	0	0	1	1	0	1	0
P63325	40S ribosomal protein S10	Rps10	1	0	0	0	0	0	0	0	0
Q69ZU8	Ankyrin repeat domain-containing protein 6	Ankrd6	1	0	0	0	0	0	0	0	0
Q6ZQ06	Centrosomal protein of 162 kDa	Cep162	1	0	0	0	0	0	0	0	0
Q8BJH1	Zinc finger C2HC domain-containing protein 1A	Zc2hc1a	1	0	0	0	0	0	0	0	0
Q9JJI8	60S ribosomal protein L38	Rpl38	1	0	0	0	0	0	0	0	0
Q62415	Apoptosis-stimulating of p53 protein 1	Ppp1r13b	0	3	2	0	0	0	0	0	0
Q9WUM5	Succinyl-CoA ligase subunit alpha (mitochondrial)	Suclg1	0	1	1	1	0	1	0	0	0
P01027	Complement C3	C3	0	1	0	0	0	0	0	0	0
P60710	Actin, cytoplasmic 1	Actb	0	1	0	0	0	0	0	0	0
Q5F2E7	Nuclear fragile X mental retardation-interacting protein 2	Nufip2	0	0	1	0	0	0	0	0	0